Article

Molecular Cell

HCF-1 Regulates *De Novo* Lipogenesis through a Nutrient-Sensitive Complex with ChREBP

Graphical Abstract

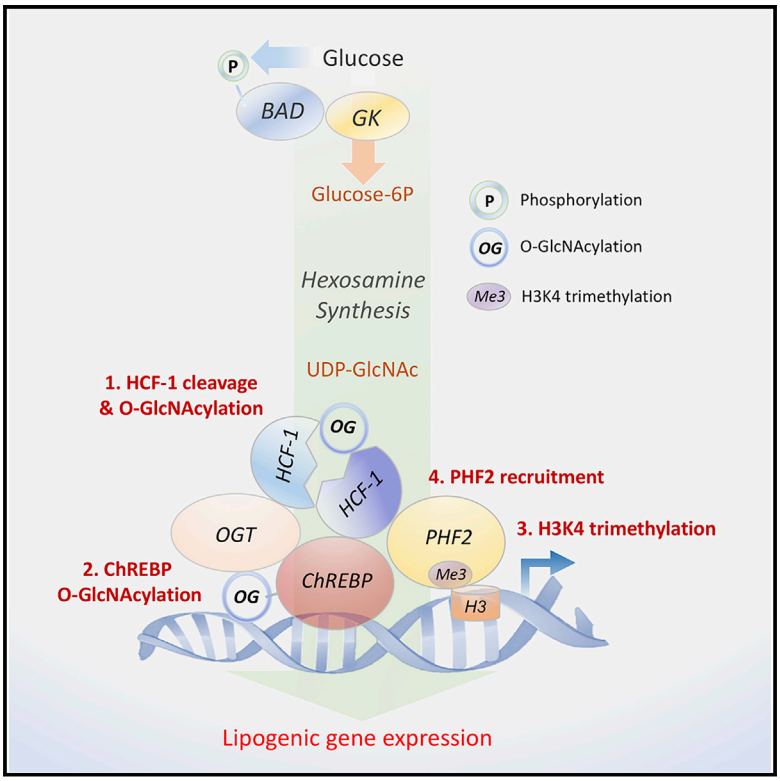

Authors

Elizabeth A. Lane, Dong Wook Choi, Luisa Garcia-Haro, Zebulon G. Levine, Meghan Tedoldi, Suzanne Walker, Nika N. Danial

Correspondence

nika_danial@dfci.harvard.edu

In Brief

Lane et al. identify HCF-1 as a ChREBP-modulatory protein relevant for *de novo* lipogenesis. Glucose stimulation triggers HCF-1 O-GlcNAcylation, priming its association with ChREBP and OGT recruitment for ChREBP O-GlcNAcylation and increased ChREBP transcriptional activity. The HCF-1:ChREBP complex imparts glucose-dependent epigenetic regulation to lipogenic promoters by recruiting epigenetic modifiers.

Highlights

- HCF-1 binds ChREBP and is required for glucose stimulation of *de novo* lipogenesis
- HCF-1 recruits OGT to ChREBP, stimulating ChREBP O-GlcNAcylation and activation
- Nutrient induction of HCF-1 O-GlcNAcylation is required for its binding to ChREBP
- HCF-1 recruits epigenetic activators to promoters of lipogenic genes

Lane et al., 2019, Molecular Cell *75*, 357–371
July 25, 2019
https://doi.org/10.1016/j.molcel.2019.05.019

CellPress

Molecular Cell
Article

HCF-1 Regulates *De Novo* Lipogenesis through a Nutrient-Sensitive Complex with ChREBP

Elizabeth A. Lane,[1,2,3,7] Dong Wook Choi,[2,3,7] Luisa Garcia-Haro,[2,3] Zebulon G. Levine,[4] Meghan Tedoldi,[2] Suzanne Walker,[4] and Nika N. Danial[2,5,6,8,*]
[1]The Biological and Biomedical Sciences Program, Harvard Medical School, Boston, MA 02115, USA
[2]Department of Cancer Biology, Dana-Farber Cancer Institute, Harvard Medical School, Boston, MA 02215, USA
[3]Department of Cell Biology, Harvard Medical School, Boston, MA 02115, USA
[4]Department of Microbiology and Immunology, Harvard Medical School, Boston, MA 02115, USA
[5]Department of Medical Oncology, Dana-Farber Cancer Institute, Harvard Medical School, Boston, MA 02115, USA
[6]Department of Medicine, Harvard Medical School, Boston, MA 02115, USA
[7]These authors contributed equally
[8]Lead Contact
*Correspondence: nika_danial@dfci.harvard.edu
https://doi.org/10.1016/j.molcel.2019.05.019

SUMMARY

Carbohydrate response element binding protein (ChREBP) is a key transcriptional regulator of *de novo* lipogenesis (DNL) in response to carbohydrates and in hepatic steatosis. Mechanisms underlying nutrient modulation of ChREBP are under active investigation. Here we identify host cell factor 1 (HCF-1) as a previously unknown ChREBP-interacting protein that is enriched in liver biopsies of nonalcoholic steatohepatitis (NASH) patients. Biochemical and genetic studies show that HCF-1 is O-GlcNAcylated in response to glucose as a prerequisite for its binding to ChREBP and subsequent recruitment of OGT, ChREBP O-GlcNAcylation, and activation. The HCF-1:ChREBP complex resides at lipogenic gene promoters, where HCF-1 regulates H3K4 trimethylation to prime recruitment of the Jumonji C domain-containing histone demethylase PHF2 for epigenetic activation of these promoters. Overall, these findings define HCF-1's interaction with ChREBP as a previously unappreciated mechanism whereby glucose signals are both relayed to ChREBP and transmitted for epigenetic regulation of lipogenic genes.

INTRODUCTION

Metabolic adaptation to fed and fasted states is intricately controlled by nutrient and hormonal signals. In the fed state, the liver stores glucose as glycogen, and when glycogen stores are replete, it converts excess glucose to fat through *de novo* lipogenesis (DNL), a process regulated by insulin and glucose-derived metabolic signals (Abdul-Wahed et al., 2017; Sanders and Griffin, 2016; Uyeda and Repa, 2006; Yecies et al., 2011). Although storage of excess glucose as lipids is an important component of metabolic adaptation, excessive DNL is associated with pathologies such as nonalcoholic fatty liver disease (NAFLD), where up to 30% of hepatic fat accumulation can be linked to increased hepatic DNL (Softic et al., 2016).

Glucose metabolism provides both biosynthetic precursors and regulatory signals for DNL, and evidence indicates that the carbohydrate response element binding protein (ChREBP) is an important transcription factor and effector of glucose-derived signals in this process (Abdul-Wahed et al., 2017; Agius, 2016a; Alves-Bezerra and Cohen, 2017; Uyeda and Repa, 2006). Notably, polymorphisms in *ChREBP* are linked to increased plasma triglycerides (Kooner et al., 2008), and increased ChREBP protein levels are associated with human NAFLD (Benhamed et al., 2012). Glucose activates ChREBP through multiple mechanisms (reviewed in Abdul-Wahed et al., 2017). For example, several glucose-derived metabolites can activate ChREBP, including G6P (glucose-6-phosphate), F2-6BP (fructose-2,6-bisphosphate) and X5P (xylulose-5-phosphate) (Arden et al., 2012; Dentin et al., 2012; Iizuka et al., 2013). There is some evidence that X5P can trigger dephosphorylation and nuclear translocation of ChREBP through activation of protein phosphatase 2A (PP2A) (Kabashima et al., 2003). However, ChREBP phosphomutants remain glucose responsive (Tsatsos and Towle, 2006), and a pool of ChREBP resides in the nucleus even in the absence of glucose stimulation (Kim et al., 2016), indicating the existence of additional glucose-dependent regulatory mechanisms. Other glucose-derived metabolic signals in the form of acetyl-coenzyme A (CoA) and uridine diphosphate -N-acetylglucosamine (UDP-GlcNAc) can activate ChREBP through acetylation and O-GlcNAcylation, respectively (Bricambert et al., 2010; Guinez et al., 2011; Sakiyama et al., 2010; Yang and Qian, 2017). Specifically, increased glucose metabolism can augment UDP-GlcNAc pools through the hexosamine biosynthesis pathway (HBP), and O-GlcNAcylation of ChREBP increases its DNA binding affinity, transcriptional activity, and protein stability (Guinez et al., 2011; Sakiyama et al., 2010; Yang et al., 2017). However, the molecular details underlying the glucose-dependent activation of ChREBP, including specific mechanisms controlling its O-GlcNAcylation, are not fully understood.

The myriad of glucose-dependent signals that converge on ChREBP reflect a complex network of mechanisms regulating gene expression in response to glucose and carbohydrate

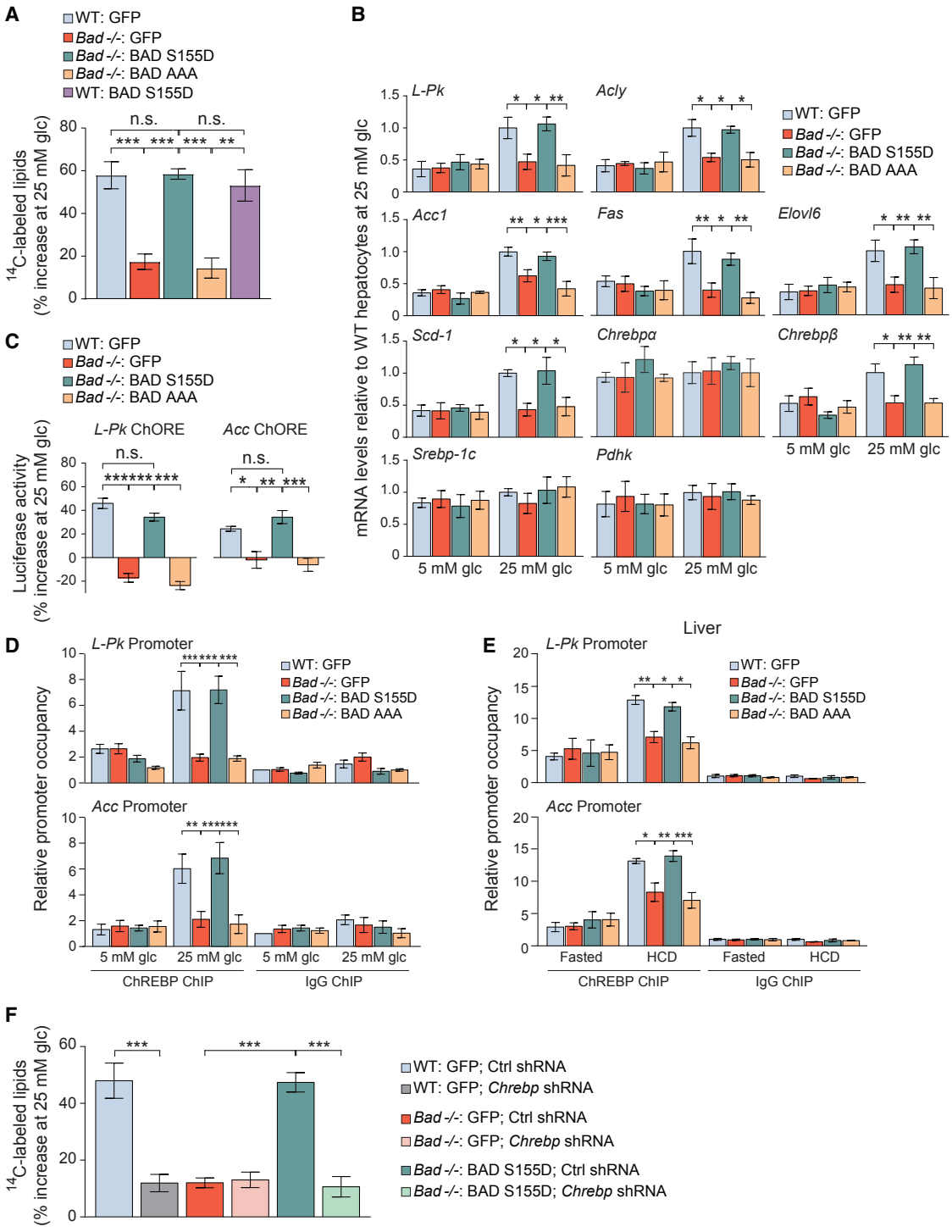

Figure 1. Altered ChREBP-Dependent *De Novo* Lipogenesis Following BAD Modifications

(A) Incorporation of glucose into lipid fractions of WT and *Bad*$^{-/-}$ hepatocytes reconstituted with the indicated adenoviruses and treated with 1 μCi of U^{14}C-glucose for 4 h. Data are presented as percent increase in label incorporation from 5–25 mM glucose (glc) treatment (n = 3–4).

(B) Relative expression of lipogenic genes in WT and *Bad*$^{-/-}$ primary hepatocytes reconstituted with the indicated adenoviruses and treated with 5 or 25 mM glucose for 20 h (n = 5). *L-PK*, liver pyruvate kinase; *Acly*, ATP citrate lyase; *Acc1*, acetyl-CoA carboxylase 1; *Fas*, fatty acid synthase; *Elovl6*, Elovl fatty acid elongase 6; *Scd-1*, stearoyl-CoA desaturase; *Chrebp*, carbohydrate response element binding protein; *Srebp-1c*, sterol regulatory element-binding protein-1$_C$; *Pdhk*, pyruvate dehydrogenase kinase.

(legend continued on next page)

surplus. In the liver, these signals are controlled by the glucose phosphorylating enzyme glucokinase (GK, hexokinase IV), the product of the maturity onset diabetes of the young type 2 (MODY2) gene (Matschinsky, 2009; Nissim et al., 2012). In the fed state, hepatic GK regulates glucose utilization and storage by stimulating glycogen and DNL while suppressing hepatic glucose production (Dentin et al., 2004; Velho et al., 1996). Genetic evidence also indicates that GK is required for activation of ChREBP by glucose and carbohydrate feeding (Dentin et al., 2004). Hepatic GK activity is regulated by a number of binding partners, including GKRP (glucokinase-regulatory protein), PFK2 or FBPase2 (6-phosphofructo-2-kinase or fructose 2,6-bisphosphatase), and BAD (BCL-2-associated agonist of cell death) (reviewed in Agius, 2016b). These endogenous modulators of GK could be components of additional signaling pathways that exert physiologic control over ChREBP activation in response to lipogenic signals. BAD activates GK when phosphorylated at serine 155 within its BH3 (BCL2 homology 3) domain downstream of the insulin signaling pathway, independent of its capacity to bind other BCL-2 family proteins (Agius, 2016b; Danial et al., 2003; Giménez-Cassina and Danial, 2015; Giménez-Cassina et al., 2014). This involves direct binding of the BAD BH3 helix near the active site of the enzyme (Szlyk et al., 2014). Activation of GK by phosphorylated BAD stimulates hepatic glucose utilization while suppressing gluconeogenesis (Giménez-Cassina et al., 2014). However, whether BAD phosphorylation is relevant to glucose stimulation of DNL is not known and could not be predicted, given the multitude of hormonal and nutrient signals that can regulate hepatic GK, ChREBP activity, and lipid synthesis. Here we show that BAD phosphorylation is necessary for glucose stimulation of DNL and utilize the BAD mutant hepatocyte system as a discovery platform to gain new molecular insights into how ChREBP is normally activated in response to glucose.

Our unbiased proteomics analyses comparing ChREBP-containing nuclear complexes in control versus BAD-deficient hepatocytes, where glucose stimulation of ChREBP is impaired, revealed host cell factor 1 (HCF-1) as a previously unknown ChREBP binding protein. A combination of biochemical, genetic, and functional studies pinpoint distinct steps at which HCF-1 modulates activation of ChREBP and the lipogenic program by glucose. In particular, formation of the HCF-1:ChREBP complex is first primed by HCF-1 glycosylation in response to glucose stimulation or carbohydrate surplus and is followed by HCF-1-dependent recruitment of GlcNAc transferase (OGT) to ChREBP and ChREBP O-GlcNAcylation. HCF-1 is also required for a glucose-stimulated increase in activating histone marks and epigenetic control of ChREBP target promoters. These data reveal shared control of ChREBP O-GlcNAcylation and activation, and epigenetic modulation of lipogenic gene promoters via HCF-1.

RESULTS

ChREBP-Dependent *De Novo* Lipogenesis Is Regulated by BAD Phosphorylation

To initially assess glucose modulation of DNL following alterations in BAD, we quantified incorporation of glucose carbons into lipid fractions of wild-type (WT) and $Bad^{-/-}$ primary hepatocytes following incubation with low (5 mM) versus high (25 mM) glucose concentrations. Compared with WT hepatocytes, the contribution of glucose to DNL was significantly lower in $Bad^{-/-}$ hepatocytes (Figure 1A). This defect was fully reversed by genetic reconstitution with the phosphomimic BAD S155D variant, capable of activating GK but not the phospho-deficient BAD AAA variant, harboring triple Ala mutations within the BAD BH3 domain (L151A, S155A, and D156A) that blunt its GK-activating capacity (Danial et al., 2008; Giménez-Cassina et al., 2014; Figures 1A and S1A). The BAD S155D and AAA mutants are particularly informative in this setting because they are deficient in binding to BCL-2 family proteins known to interact with the BAD BH3 domain (Danial et al., 2008; Giménez-Cassina et al., 2014). This enabled assessment of the GK-activating property of BAD without the confounding effects of other BAD-interacting proteins. In WT hepatocytes, BAD S155D did not lead to additional augmentation of lipogenesis beyond the level seen in GFP-expressing controls (Figure 1A), indicating that, at least in this acute setting, phospho-BAD does not lead to hyper-stimulation of the lipogenic program by glucose.

Hepatic lipogenesis is substantially regulated at the transcriptional level by the sterol regulatory element-binding protein-1_C (SREBP-1_C) and ChREBP transcription factors, which have overlapping target genes and mediate the input from insulin and glucose, respectively (Abdul-Wahed et al., 2017; Agius, 2016b; Herman et al., 2012; Uyeda and Repa, 2006; Wang et al., 2015; Yecies et al., 2011). Because our primary focus was on regulation of lipogenesis by glucose, we performed all subsequent measurements in hepatocytes in response to glucose alone without insulin stimulation (Petrie et al., 2013). As expected, a substantial increase in the mRNA abundance of lipogenic genes was observed upon glucose stimulation of WT hepatocytes (Figures 1B and S1B). *Chrebp*α mRNA levels were not substantially regulated by glucose, but those of the *Chrebp*β isoform were induced (Figure 1B), which is consistent with previous reports (Herman et al., 2012; Stamatikos et al., 2016). In BAD-deficient hepatocytes, glucose induction of mRNAs for lipogenic genes was significantly blunted (Figure 1B). However,

(C) ChoRE luciferase reporter activity in WT and $Bad^{-/-}$ primary hepatocytes treated as in (B). Data are represented as percent increase in reporter activity upon glucose stimulation (n = 4).

(D) Relative occupancy of ChREBP at *L-Pk* and *Acc* promoters in WT and $Bad^{-/-}$ primary hepatocytes reconstituted with the indicated adenoviruses and treated with 5 or 25 mM glucose for 4 h (n = 7).

(E) Relative occupancy of ChREBP at the promoters of *L-Pk* and *Acc* in livers of WT and $Bad^{-/-}$ mice reconstituted with the indicated adenoviruses 1 week prior to being fasted for 24 h and refed a HCD for 18 h (n = 3–4).

(F) DNL assays in WT and $Bad^{-/-}$ hepatocytes co-infected with the indicated adenoviruses and assessed as in (A) (n = 4).

Error bars in (A)–(F) are means ± SEM. *p < 0.05; **p < 0.01; ***p < 0.001; n.s., non-significant; one-way ANOVA (A, C, and F) or two-way ANOVA (B, D, and E). See also Figures S1 and S2 and Table S1.

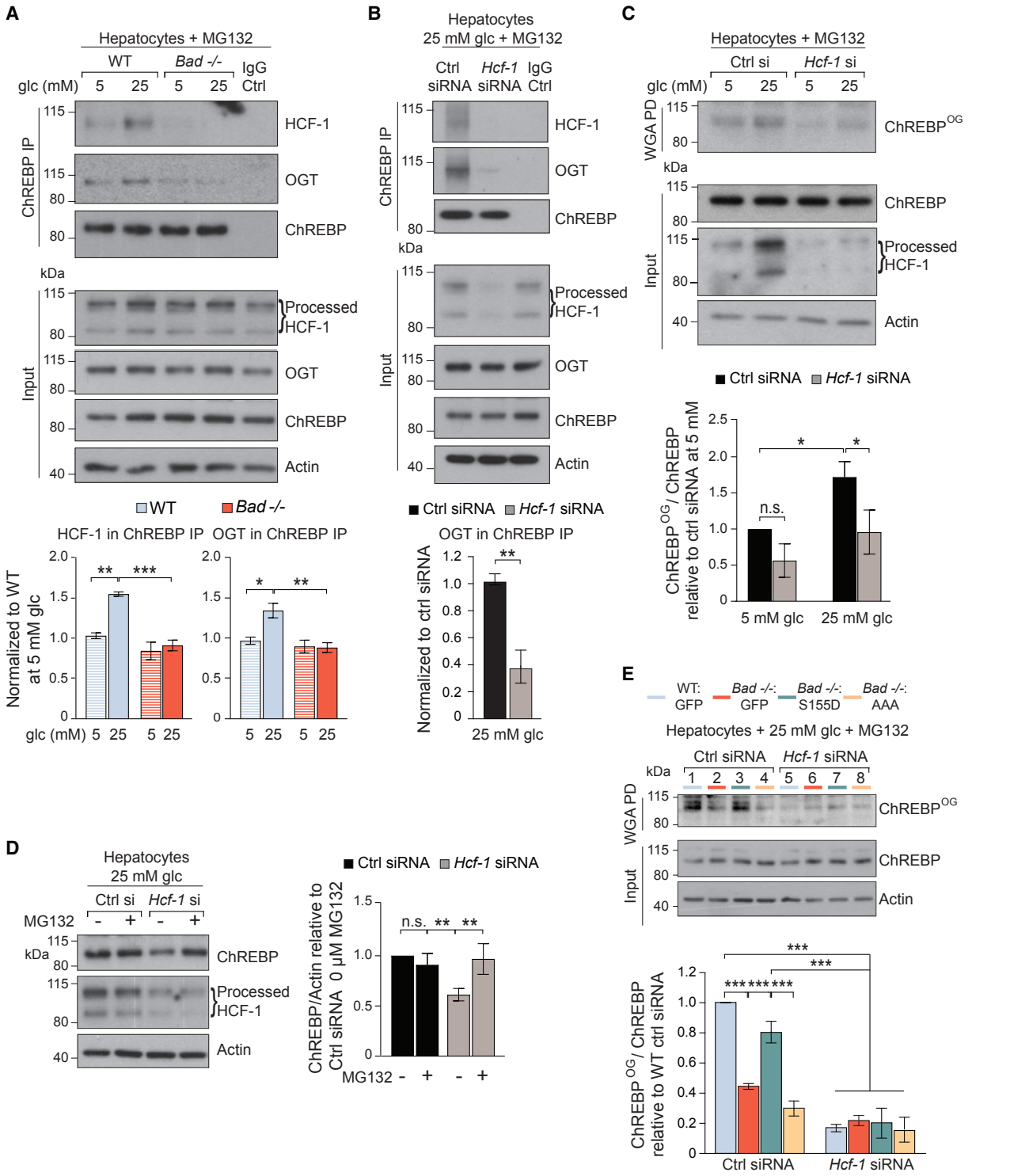

Figure 2. HCF-1 Interacts with ChREBP and Is Required for Its O-GlcNAcylation

(A) Representative western blots (top) and quantification by densitometry of 4 experiments (bottom) of ChREBP association with HCF-1 and OGT in WT and *Bad*$^{-/-}$ primary hepatocytes cultured in 5 or 25 mM glucose for 6 h in the presence of 20 μM MG132.

(B) Representative western blots (top) and quantification of 3 experiments (bottom) of ChREBP association with HCF-1 and OGT following *Hcf-1* knockdown in WT hepatocytes cultured in 25 mM glucose for 6 h in the presence of 20 μM MG132.

(legend continued on next page)

the expression of other genes whose transcription is not glucose responsive, such as *Chrebp*α, *Srebp-1*$_C$, and pyruvate dehydrogenase kinase (*Pdhk*) (Stamatikos et al., 2016; Zhang et al., 2015), was comparable with WT hepatocytes stimulated with glucose (Figure 1B). As in lipogenesis assays (Figure 1A), BAD S155D, but not AAA, restored glucose induction of lipogenic gene transcripts in *Bad*$^{-/-}$ hepatocytes (Figure 1B). Importantly, BAD S155D does not rescue lipogenic gene expression in *Bad*$^{-/-}$ hepatocytes subjected to *Gk* knockdown (Figure S1C). Likewise, BAD S155D does not rescue lipogenic gene expression in GK-deficient hepatocytes, which, similar to *Bad*$^{-/-}$ hepatocytes, display a defect in glucose stimulation of DNL gene expression (Dentin et al., 2004; Figure S1D). Collectively, these observations, together with the deficiency of the non-GK-activating BAD AAA mutant in stimulating DNL in response to glucose, indicate that the effect of phospho-BAD requires an intact GK. BAD-dependent changes in lipogenic gene expression are associated with altered ChREBP activity, as evident from two complementary functional readouts; luciferase reporters containing the carbohydrate response elements (ChoREs) of the *L-Pk* and *Acc* genes and chromatin immunoprecipitation (ChIP) assays examining promoter occupancy of ChREBP at target genes. Glucose induction of ChoRE reporters and recruitment of ChREBP to endogenous promoters of the *L-Pk* and *Acc* genes were significantly lower in *Bad*$^{-/-}$ compared with WT primary hepatocytes but were restored to WT levels following genetic rescue with the GK-activating BAD S155D but not the BAD AAA mutant (Figures 1C and 1D).

As an *in vivo* correlate to our findings in hepatocyte cultures, we also examined hepatic ChREBP activity and the lipogenic gene program in liver biopsies from WT and *Bad*$^{-/-}$ mice subjected to short-term (18-h) high-carbohydrate diet (HCD) feeding, a treatment known to activate hepatic ChREBP (Agius, 2016a). ChREBP binding to *L-Pk* and *Acc* gene promoters as well as transcriptional induction of lipogenic genes in response to HCD were significantly attenuated in *Bad*$^{-/-}$ liver (Figures 1E and S1E). Hepatic reconstitution of *Bad*$^{-/-}$ mice with BAD S155D or AAA corroborated our findings in primary hepatocytes that full induction of ChREBP activity and lipogenic gene expression require BAD phosphorylation (Figures 1E, S1E, and S1F). Notably, BAD S155 phosphorylation is normally induced in the liver upon HCD feeding or in primary hepatocytes following glucose stimulation (Figures S1G and S1H). Thus, BAD phosphorylation is a downstream effector of lipogenic signals that converge on ChREBP activation.

To establish a cause-and-effect relationship between phospho-BAD and ChREBP activity, we tested the effects of BAD S155D on DNL in the context of ChREBP deficiency. *Chrebp* knockdown in WT primary hepatocytes led to diminished DNL and transcriptional induction of lipogenic genes in response to glucose, consistent with previous reports (Dentin et al., 2006), and completely ablated the ability of BAD S155D to restore lipogenesis in *Bad*$^{-/-}$ hepatocytes (Figures 1F, S2A, and S2B). In *Bad*$^{-/-}$ hepatocytes, ChREBP depletion had no additional effect on reducing DNL (Figure 1F). Taken together, these data indicate that the effect of phospho-BAD on glucose stimulation of lipogenesis is mediated by ChREBP. Thus, although BAD is one of many GK-modulatory mechanisms in the liver, its modification is sufficient to alter glucose stimulation of ChREBP activity and DNL.

Identification of HCF-1 as a ChREBP Binding and Regulatory Protein

We next took advantage of WT and *Bad*$^{-/-}$ hepatocytes, in which glucose induction of ChREBP is preserved or blunted, as an unbiased discovery platform to learn about new biochemical mechanisms that can contribute to glucose regulation of ChREBP. To this end, we initially examined changes in ChREBP-containing protein complexes in glucose-stimulated WT hepatocytes compared with BAD-deficient counterparts using immunoprecipitation (IP) coupled to mass spectrometry (MS). ChREBP was immunoprecipitated from the nuclear fractions of primary WT and *Bad*$^{-/-}$ hepatocytes expressing FLAG-tagged ChREBP and cultured in 25 mM glucose. Among proteins captured by the anti-FLAG antibody in WT hepatocytes were known ChREBP binding proteins such as Max-like protein X (Mlx), an obligate partner of ChREBP (Ma et al., 2006; Figures S3A–S3C). We then prioritized candidates that were $\geq$3-fold more abundant in ChREBP IPs in WT compared with *Bad*$^{-/-}$ hepatocytes and focused on proteins with direct or indirect functional annotations in gene transcription and glucose signaling by gene ontology, STRING, and DAVID bioinformatic tools. Using this filtering approach, the only protein with known roles in both transcription and glucose signaling was HCF-1, which was enriched by 3.5-fold in ChREBP IPs of WT compared with *Bad*$^{-/-}$ samples (Figures S3B and S3D). HCF-1 is a transcriptional co-regulator whose interaction with ChREBP or role in DNL has not been reported previously. HCF-1 is proteolytically processed by OGT at multiple cleavage sites, which produces N- and C-terminal fragments that remain non-covalently bound, forming a conformation that is important for HCF-1 function (Capotosti et al., 2011; Daou et al., 2011; Janetzko et al., 2016; Lazarus et al., 2013).

We next validated the association of endogenous ChREBP and HCF-1 in WT hepatocytes and confirmed that it was diminished in the absence of BAD (Figure 2A). These experiments were performed in the presence of the proteasome inhibitor MG132 to normalize ChREBP protein stability (Guinez et al.,

(C) Representative western blots (top) and quantification of 3 experiments (bottom) of O-GlcNAcylated ChREBP (ChREBP^{OG}) in wheat germ agglutinin (WGA) pull-down (PD) assays in WT hepatocytes subjected to *Hcf-1* knockdown and cultured as in (A).

(D) Representative western blots (left) and quantification of 3 experiments (right) of ChREBP protein levels in WT hepatocytes subjected to *Hcf-1* knockdown and cultured in 25 mM glucose for 6 h in the absence or presence of 20 μM MG132.

(E) Representative western blots (top) and quantification of 3 experiments (bottom) of ChREBP^{OG} in primary WT and *Bad*$^{-/-}$ hepatocytes reconstituted with the indicated BAD mutants, subjected to *Hcf-1* knockdown, and cultured in 25 mM glucose for 6 h in the presence or absence of 20 μm MG132.

Error bars are means ± SEM. *p < 0.05, **p < 0.01, ***p < 0.001; n.s., non-significant; two-way ANOVA (A and C–E) or one-way ANOVA (B). See also Figures S3 and S4.

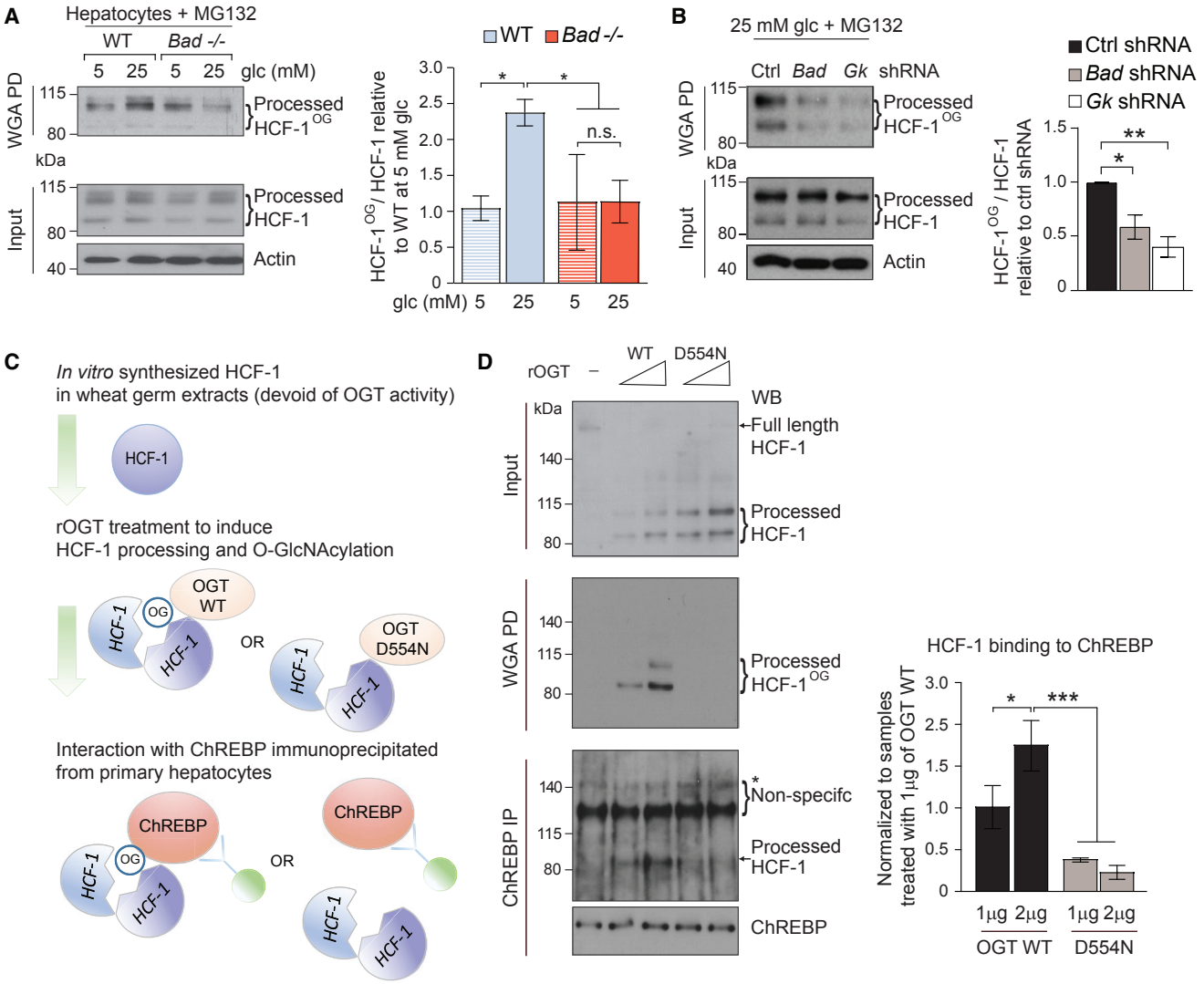

(legend on next page)

2011) because endogenous ChREBP levels were found to be lower in *Bad*$^{-/-}$ hepatocytes and liver compared with WT controls (see below). Notably, the association of HCF-1 and ChREBP in WT hepatocytes and liver samples is induced in response to glucose stimulation or HCD, respectively (Figures 2A and S3E). To our knowledge, this is the first example of an HCF-1-containing protein complex that is induced by nutrient stimulation. In comparison, the HCF-1:PGC1α complex is enriched only at low or basal glucose concentrations or in the fasted state in hepatocytes and liver (Ruan et al., 2012), and other HCF-1-containing complexes are not known to be nutrient responsive (Mazars et al., 2010; Thomas et al., 2016; Tyagi et al., 2007).

HCF-1 is first and foremost known as a transcriptional co-regulator; however, in limited settings, it may facilitate protein Ser and/or Thr O-GlcNAcylation by recruiting OGT to specific partner proteins (Han et al., 2017; Ruan et al., 2012). This adaptor-like function of HCF-1 has been demonstrated in the context of two interacting partners, PGC1α and NRF1 (Han et al., 2017; Ruan et al., 2012), and remains to be further studied. In addition to HCF-1, OGT was also present in ChREBP immunoprecipitates in a glucose- and HCD-responsive manner (Figures 2A and S3E). Notably, depletion of HCF-1 in WT hepatocytes led to diminished capture of OGT in ChREBP immunoprecipitates (Figure 2B), indicating that HCF-1 is required for recruitment of OGT to ChREBP. Consistent with these observations, HCF-1 depletion also led to decreased ChREBP O-GlcNAcylation (ChREBP^{OG}) in response to 25 mM glucose (Figures 2C, S4A, and S4B). Reduced ChREBP O-GlcNAcylation in this setting was commensurate with lower ChREBP protein levels (Figures 2D and S4B), consistent with reports that ChREBP stability is regulated by O-GlcNAcylation (Guinez et al., 2011; Sakiyama et al., 2010). Under conditions where glucose stimulation of ChREBP activity is blunted, as in the absence of GK or BAD, the interaction between HCF-1 and OGT with ChREBP is significantly diminished in response to glucose stimulation or HCD (Figures 2A, S3E, S4C, and S4D). This parallels a corresponding decrease in ChREBP^{OG} and ChREBP protein levels in *Bad*$^{-/-}$ hepatocytes, which were rescued with BAD S155D but not BAD AAA (Figures 2E, lanes 1–4, S4E, and S4F). Notably, BAD S155D was ineffective in the context of *Hcf-1* knockdown (Figures 2E, lane 3 versus lane 7, and S4F), further corroborating the necessity of HCF-1 for ChREBP O-GlcNAcylation. Collectively, our findings indicate that HCF-1 is a ChREBP binding partner required for recruitment of OGT to ChREBP and ChREBP O-GlcNAcylation in a glucose- and HCD-sensitive protein complex.

HCF-1 O-GlcNAcylation Is Induced by Lipogenic Signals and Selectively Regulates Its Interaction with ChREBP

OGT modifies HCF-1 both through proteolytic cleavage, which proceeds via intermediary non-canonical glutamate side-chain glycosylation, and through canonical O-GlcNAcylation of Ser and/or Thr residues (Janetzko et al., 2016). However, whether HCF-1 glycosylation is regulated by nutrient stimulation and dietary treatment has not been examined previously. This is a relevant question because factors beyond UDP-GlcNAc levels can regulate protein O-GlcNAcylation, as evident from preferential O-GlcNAcylation of some OGT substrates under conditions where UDP-GlcNAc levels are reduced (Ruan et al., 2012; Taylor et al., 2009; Yang and Qian, 2017). Therefore, HCF-1 O-GlcNAcylation may not necessarily be responsive to nutrient fluctuations. However, we found that HCF-1 O-GlcNAcylation is significantly increased in primary hepatocytes in response to glucose stimulation and in liver derived from HCD-treated mice (Figures 3A and S5A). Moreover, HCF-1 O-GlcNAcylation in response to glucose or HCD is blunted in BAD-deficient hepatocytes or in hepatocytes subjected to acute knockdown of *Gk* or *Bad* (Figures 3A, 3B, and S5A). Notably, this defect can be rescued by BAD S155D in a GK-dependent manner (Figures S5B and S5C). Collectively, these data further corroborate the sensitivity of HCF-1 glycosylation to changes in glucose metabolism.

To date, no functional roles have been ascribed to HCF-1 Ser and/or Thr O-GlcNAcylation, motivating us to investigate whether this modification is required for HCF-1 binding to ChREBP. To this end, we incubated *in vitro* transcribed and translated HCF-1 with increasing amounts of recombinant WT OGT or the OGT D554N mutant shown previously to be selectively impaired in canonical Ser and/or Thr O-GlcNAcylation but not HCF-1 proteolytic cleavage (Janetzko et al., 2016; Figures 3C, 3D, and S5D). This enabled generation of two HCF-1 variants that underwent proteolytic processing (Figure 3D, input), but differed in O-GlcNAcylation (Figure 3D, wheat germ agglutinin [WGA] pull-down [PD]). Proteolytic processing of HCF-1 by the OGT D554N mutant was more efficient compared with WT OGT, consistent with a published characterization of this mutant (Janetzko et al., 2016). We then examined the capacity of these differentially O-GlcNAcylated HCF-1 proteins to interact with ChREBP that was immunoprecipitated from primary hepatocytes and found that HCF-1 processed by the OGT D554N mutant is significantly impaired in ChREBP binding compared

Figure 3. HCF-1 O-GlcNAcylation Selectively Regulates Its Association with ChREBP

(A) Representative western blots (left) and quantification of 3 experiments (right) of HCF-1^{OG} in WT and *Bad*$^{-/-}$ primary hepatocytes cultured in 5 or 25 mM glucose for 6 h in the presence of 20 μM MG132.

(B) Representative western blots (left) and quantification of 3 experiments (right) of HCF-1^{OG} in WT primary hepatocytes subjected to *Bad* or *Gk* knockdown and cultured in 25 mM glucose for 6 h in the presence of 20 μM MG132.

(C and D) Schematic of the experimental system to generate glycosylated or non-glycosylated recombinant HCF-1 and test its interaction with ChREBP (C). Representative western blots (left) and quantification of 3 experiments (right) show the interaction between recombinant HCF-1 generated as in (C) and ChREBP (D). rOGT, recombinant OGT.

(E and F) Interaction of FLAG-tagged ChREBP (E) compared with FLAG-tagged PGC1α (F) with differentially glycosylated HCF-1 in 293T cells transfected with OGT WT or D554N.

Error bars in (A), (B), and (D)–(F) are means ± SEM. *$p < 0.05$, **$p < 0.01$, ***$p < 0.001$; n.s., non-significant; two-way ANOVA (A and D) or one-way ANOVA (B, E, and F). See also Figure S5.

with HCF-1 processed by WT OGT (Figure 3D, ChREBP IP). Collectively, these data indicate that HCF-1 glycosylation is required for its binding to ChREBP and is stimulated by lipogenic signals, providing a biochemical explanation for the observed enrichment of the ChREBP:HCF-1 complex in response to glucose stimulation or HCD treatment (Figures 2A and S3E).

To determine whether HCF-1 glycosylation is generally relevant for its binding interactions or a specific requirement for its association with ChREBP, we also examined the effect of HCF-1 O-GlcNAcylation on its capacity to bind PGC1α. To this end, we expressed FLAG-tagged PGC1α or ChREBP and either WT or D554N OGT in 293T cells. As with the above *in vitro* system, HCF-1 was comparably cleaved by WT and D554N OGT but differentially glycosylated in 293T cells (Figures 3E and 3F). In comparison with the *in vitro* system, where HCF-1 glycosylation was undetectable in the presence of OGT D554N (Figure 3D), basal HCF-1 glycosylation could be detected in 293T cells expressing this mutant, likely because of endogenous OGT activity (Figures 3E and 3F). Nonetheless, expression of WT OGT produced a larger increase in HCF-1 glycosylation and, unlike the D554N OGT mutant, led to higher capture of HCF-1 in FLAG-ChREBP immunoprecipitates (Figure 3E). In contrast, HCF-1 was captured equally in FLAG-PGC1α immunoprecipitates from cells expressing WT or D554N mutant OGT (Figure 3F). These data indicate that, unlike its interaction with ChREBP, HCF-1 interaction with PGC1α is insensitive to the HCF-1 glycosylation status. These findings establish a specific biochemical function of HCF-1 Ser and/or Thr O-GlcNAcylation by demonstrating its selective requirement for ChREBP binding and reveal HCF-1 glycosylation as a molecular mechanism dictating the specificity of HCF-1 and ChREBP interaction.

Regulation of ChREBP by HCF-1 Is Sensitive to Changes in the HBP

Our findings suggest that lipogenic signals or alterations in glucose metabolism regulate HCF-1-dependent recruitment of OGT to ChREBP, modulating its glycosylation. Beyond OGT recruitment, it is possible that changes in the OGT substrate UDP-GlcNAc also regulate this process. However, individual OGT substrates have differential sensitivity to fluctuations in UDP-GlcNAc levels (Shen et al., 2012). Thus, the extent to which HCF-1 O-GlcNAcylation and its binding to ChREBP, which requires HCF-1 to be glycosylated (Figures 3D-E), might be sensitive to changes in HBP and UDP-GlcNAc levels is not evident. To address this question, we utilized *Bad*$^{-/-}$ hepatocytes as a model system where HBP metabolites were found to be lower in response to glucose stimulation, commensurate with diminished HCF-1 glycosylation and association with ChREBP without global diminution in protein O-GlcNAcylation (Figure 4A, Table S2; data not shown). HBP metabolites were rescued by genetic reconstitution of *Bad*$^{-/-}$ hepatocytes with BAD S155D but not BAD AAA, in keeping with phospho-BAD-dependent modulation of GK activity and hepatic glucose metabolism (Giménez-Cassina et al., 2014; Figure 4A). We reasoned that if lower UDP-GlcNAc levels contribute to diminished HCF-1 glycosylation in this setting, then supplementation with HBP metabolites should rescue HCF-1 O-GlcNAcylation. To test this possibility, we used GlcNAc or glucosamine (GlcN), which bypasses the rate-limiting reaction catalyzed by glutamine-fructose-6-phosphate aminotransferase (GFAT) to enter the HBP upon direct phosphorylation (Guinez et al., 2011) and found that both were sufficient to restore HCF-1 O-GlcNAcylation in *Bad*$^{-/-}$ hepatocytes (Figures 4B and S6A). Remarkably, HBP metabolite supplementation was also sufficient to fully rescue the interaction between ChREBP with HCF-1 and OGT in this setting (Figures 4C and S6B). This is in keeping with the finding that HCF-1 glycosylation regulates its binding to ChREBP (Figures 3D and 3E). Metabolite rescue of this HCF-1- and OGT-containing ChREBP complex was accompanied by restoration of ChREBP O-GlcNAcylation and ChREBP protein levels and target gene activation in response to glucose stimulation (Figures S6C–S6E). These results are significant because they indicate that HCF-1 O-GlcNAcylation and the attendant HCF-1:ChREBP complex formation are sensitive to glucose modulation of UDP-GlcNAc pools.

We next examined the extent to which the lipogenic program is reinstated by GlcNAc supplementation of *Bad*$^{-/-}$ hepatocytes beyond restoration of ChREBP transcriptional activity. We found that GlcNAc treatment led to significant rescue of the biochemical defect in lipogenesis (Figure 4D). Although significant, rescue of lipogenesis was partial, despite full restoration of ChREBP O-GlcNAcylation and lipogenic gene expression (Figures 4D, S6C, and S6E). This may reflect the requirement of multiple branchpoints of glucose metabolism downstream of GK for induction of DNL beyond glucose stimulation of ChREBP activity. These include malonyl-CoA, produced downstream of the glycolytic and oxidative arms of glucose metabolism, as well as NADPH, generated through the pentose phosphate pathway, which are not expected to be restored by GlcNAc treatment (Alves-Bezerra and Cohen, 2017; Sanders and Griffin, 2016).

ChREBP-Dependent Binding of HCF-1 to Lipogenic Gene Promoters Is Required for Recruitment of the Epigenetic Activator PHF2

The finding that HCF-1 is required for ChREBP O-GlcNAcylation warranted more detailed examination of its role in DNL. In WT primary hepatocytes, glucose incorporation into lipids and lipogenic gene expression were significantly impaired in response to glucose following *Hcf-1* knockdown (Figures 5A and 5B). ChIP assays further indicated that, similar to ChREBP, HCF-1 is normally recruited to lipogenic gene promoters in response to glucose stimulation (Figure 5C). HCF-1 does not contain a DNA binding domain; however, its recruitment to lipogenic gene promoters is mediated by ChREBP, as evident from diminution of the HCF-1 ChIP signal in WT hepatocytes subjected to *Chrebp* knockdown (Figure 5D). Similarly, in *Bad*$^{-/-}$ hepatocytes, where the HCF-1:ChREBP complex is at low abundance, HCF-1 recruitment to lipogenic gene promoters is significantly blunted (Figure 5C).

ChREBP has been shown recently to recruit the epigenetic coactivator plant homeodomain finger 2 (PHF2), also known as KDM7C, which, in turn, demethylates inhibitory H3K9me2 marks at the promoters of ChREBP target genes to enhance transcription (Bricambert et al., 2018). This prompted examination of whether PHF2 is a component of the ChREBP:HCF-1 promoter complex. HCF-1 immunoprecipitation assays indicated that, in addition to ChREBP, PHF2 interacts with HCF-1 in primary hepatocytes and that this association is enriched in response

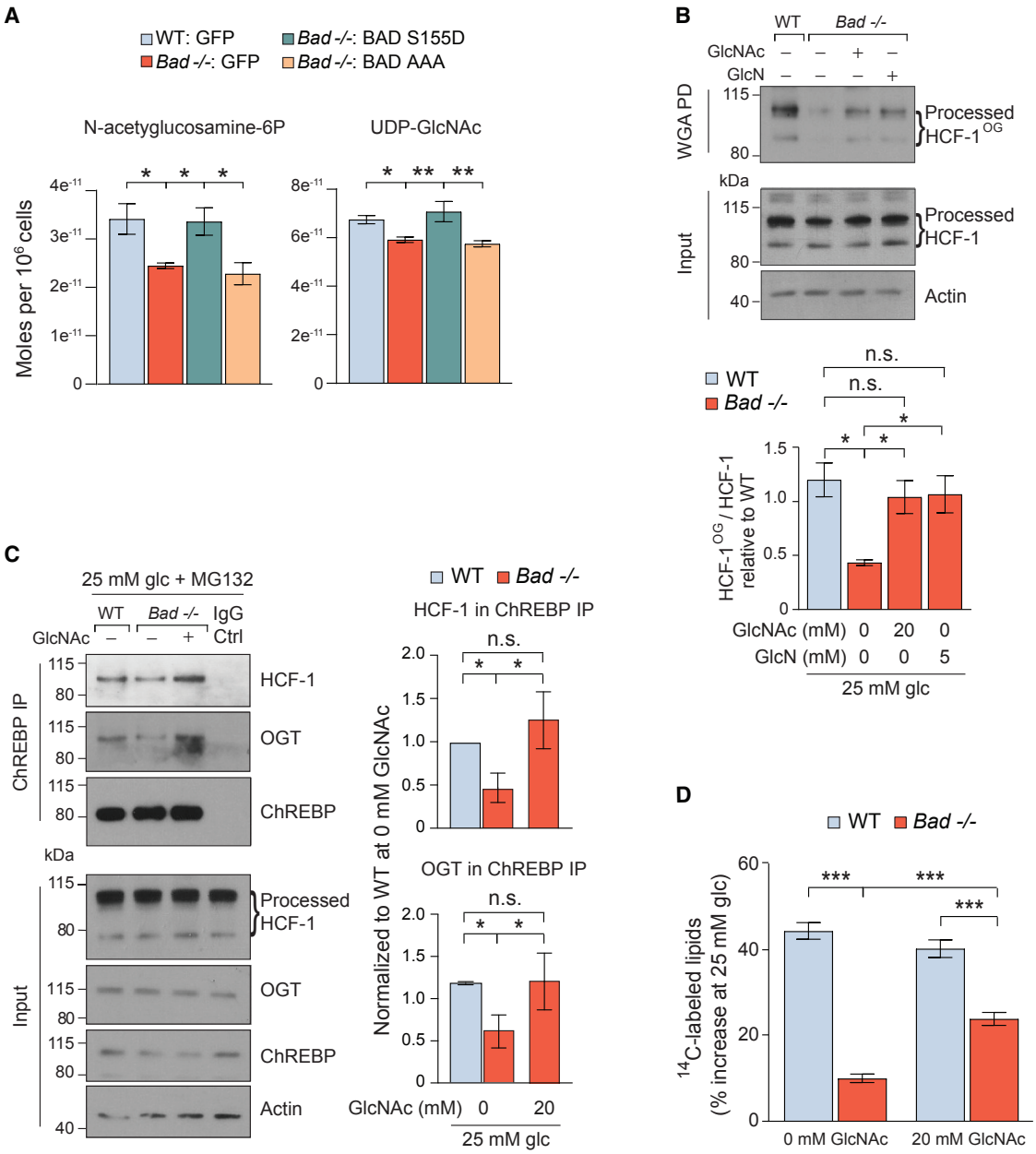

Figure 4. Regulation of the HCF-1:ChREBP Complex by Hexosamine Pathway Metabolites

(A) Liquid chromatography (LC)-mass spectrometry (MS) quantification of N-acetyglucosamine-6-phosphate and UDP-GlcNAc in WT and *Bad*$^{-/-}$ primary hepatocytes reconstituted with the indicated adenoviruses and cultured in 25 mM glucose for 5 h (n = 4–8).

(B) Representative western blots (top) and quantification of 3 experiments (bottom) of HCF-1^{OG} in WT and *Bad*$^{-/-}$ primary hepatocytes cultured in 25 mM glucose (glc) and 20 μM MG132 in the absence or presence of 20 mM GlcNAc or 5 mM GlcN for 6 h.

(C) Representative western blots (left) and quantification of 3 experiments (right) of ChREBP association with HCF-1 and OGT in WT and *Bad*$^{-/-}$ primary hepatocytes cultured in the absence or presence of GlcNAc as in (B).

(D) DNL assays in WT and *Bad*$^{-/-}$ hepatocytes cultured in the absence or presence of 20 mM GlcNAc and assessed as in Figure 1A (n = 4).

Error bars are means ± SEM. *p < 0.05, **p < 0.01, ***p < 0.001; two-way ANOVA. See also Figure S6 and Table S2.

to glucose stimulation (Figure 5E). The interaction between ChREBP and PHF2 is sensitive to GlcNAc levels, as evident from the observation that this complex is reduced in *Bad*$^{-/-}$ hepatocytes treated with 25 mM glucose and rescued upon GlcNAc supplementation, similar to ChREBP and HCF-1 interaction (Figure S7). Remarkably, *Hcf-1* knockdown in WT hepatocytes leads to diminished association between ChREBP and PHF2 and inhibits the recruitment of PHF2 to lipogenic gene promoters (Figures 5F and 5G). This indicates that PHF2 recruitment to ChREBP-containing promoter complexes is mediated by

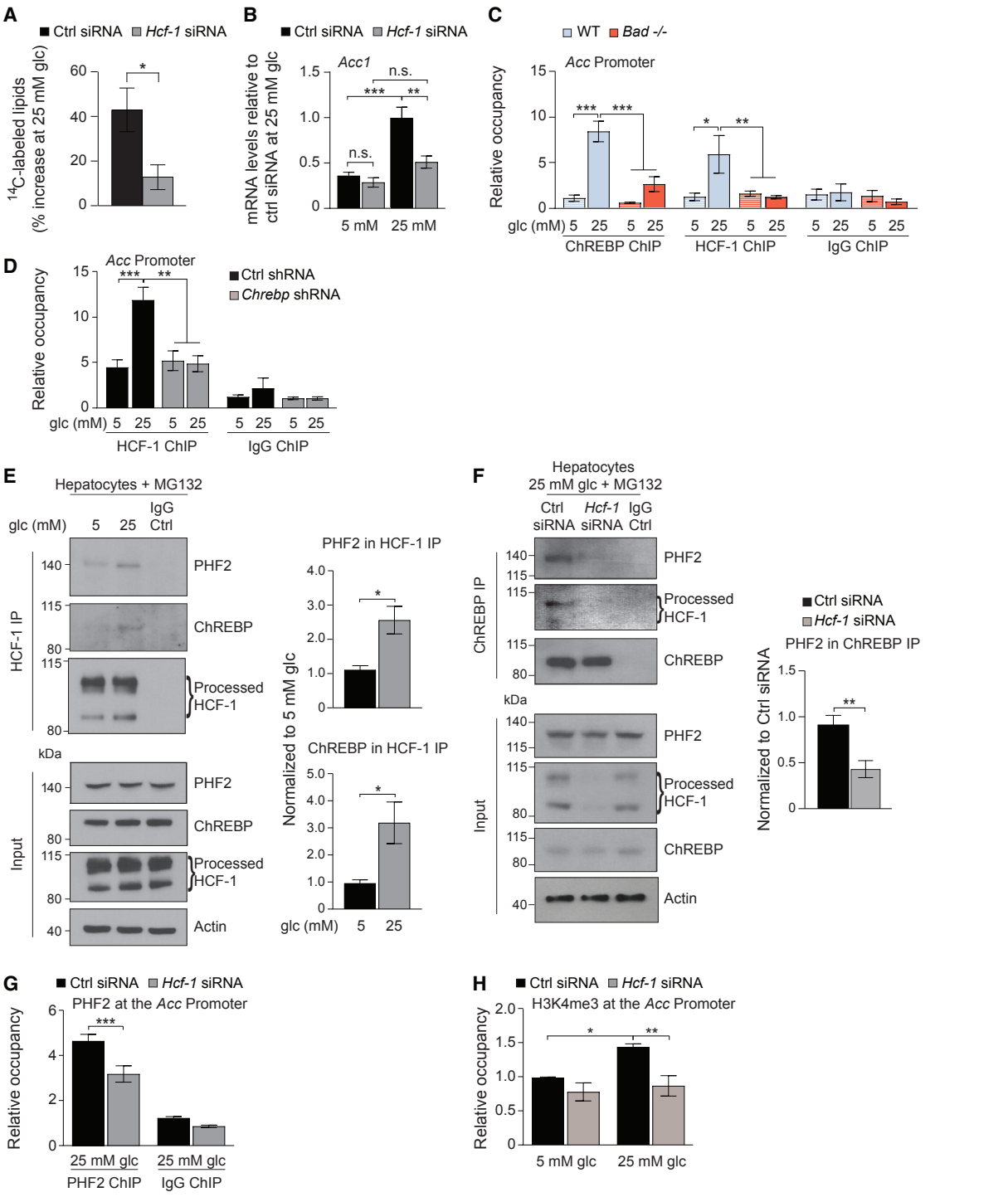

Figure 5. HCF-1 Binds to the Promoters of Lipogenic Genes in a ChREBP-Dependent Manner and Is Required for Recruitment of PHF2

(A) DNL assays in primary hepatocytes subjected to *Hcf-1* knockdown and assessed as in Figure 1A (n = 3).

(B) Relative expression of *Acc* in primary hepatocytes subjected to *Hcf-1* knockdown and treated with 5 or 25 mM glucose for 20 h (n = 3).

(C) Relative occupancy of ChREBP and HCF-1 at the *Acc* promoter in WT and *Bad*$^{-/-}$ primary hepatocytes treated with 5 or 25 mM glucose for 4 h (n = 9 experimental repeats in hepatocytes derived from 3 mice per genotype).

(D) Relative occupancy of HCF-1 at the *Acc* promoter in primary hepatocytes subjected to *Chrebp* knockdown and treated with 5 or 25 mM glucose for 4 h (n = 6 experimental repeats in hepatocytes derived from 3 mice per genotype).

(legend continued on next page)

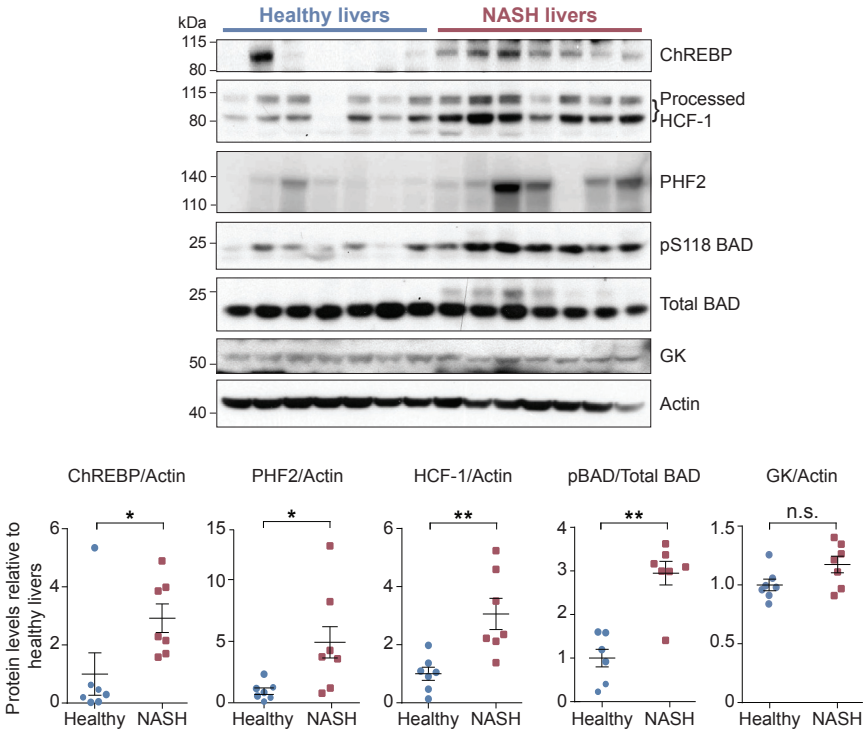

Figure 6. Increased HCF-1 Levels in Livers of Human NASH Patients

Immunoblot analysis (top) and quantification (bottom) of the indicated proteins in liver biopsies from healthy subjects and NASH patients (n = 7). Error bars are means ± SEM. *p < 0.05, **p < 0.01, n.s., non-significant; Student's t test. See also Table S3.

HCF-1 Levels in NASH Liver Biopsies

Under normal physiological conditions, human hepatic DNL is kept at low levels (Sanders and Griffin, 2016). However, excessive DNL can contribute to hepatic steatosis in response to carbohydrate overload and in NAFLD (Softic et al., 2016). The relevance of ChREBP in fatty liver disease is highlighted by studies showing that ChREBP overexpression in mice leads to hepatic steatosis and that ChREBP proteins levels are elevated in livers of humans with NAFLD (Benhamed et al., 2012; Dentin et al., 2006; Hurtado del Pozo et al., 2011). Identification of HCF-1 as a ChREBP binding protein required for lipogenic gene expression prompted assessment of HCF-1 in a pathologic setting of excessive hepatic DNL, as in human patients with fatty liver. ChREBP and PHF2 protein levels were higher in NASH (nonalcoholic steatohepatitis) patients compared with healthy liver donors, consistent with previous reports (Figure 6; Table S3; Bricambert et al., 2018). Remarkably, HCF-1 levels were significantly enriched in NASH liver biopsies along with BAD phosphorylation on S118 (equivalent to S155 in the mouse BAD sequence) (Figure 6). These data, in conjunction with our findings that HCF-1 regulates ChREBP, suggest that the HCF-1-ChREBP biochemical axis, including its regulation by phospho-BAD, may be relevant in the pathophysiology of fatty liver disease. This possibility awaits future investigation of the consequences of hepatic HCF-1 alterations in mouse models of fatty liver.

HCF-1 and, together with the data in Figure 5D, suggests a previously unappreciated tiered promoter recruitment process whereby ChREBP recruits HCF-1 to lipogenic promoters, which, in turn, recruit PHF2.

PHF2 binds H3K4me3 histone tails, and H3K4me3 is a key histone mark, priming PHF2 recruitment to transcriptionally active promoters (Bricambert et al., 2018). The finding that HCF-1 is required for binding of PHF2 to lipogenic gene promoters warranted examination of whether HCF-1 modulates H3K4me3 at these promoters, facilitating PHF2 recruitment. We directly examined this possibility using H3K4me3 ChIP assays comparing hepatocytes subjected to control versus *Hcf-1* knockdown. In contrast to control hepatocytes, where glucose stimulation augments H3K4me3 at lipogenic gene promoters, this histone modification was significantly lower in HCF-1-depleted hepatocytes (Figure 5H). Thus, the necessity of HCF-1 for PHF2 recruitment to lipogenic gene promoters is consistent with HCF-1-dependent modulation of H3K4 trimethylation. Overall, these findings suggest that HCF-1 modulation of lipogenic gene transcription is linked to epigenetic regulation of ChREBP target promoters.

DISCUSSION

Our studies uncover an intricate interplay between lipogenic signals and transcriptional activation of hepatic DNL via stepwise assembly of an active promoter complex containing ChREBP

(E) Representative western blots (left) and quantification of 3 experiments (right) of HCF-1 association with ChREBP and PHF2 in primary hepatocytes cultured in 5 or 25 mM glucose for 6 h in the presence of 20 μM MG132.

(F) Representative western blots (left) and quantification of 5 experiments (right) of ChREBP association with PHF2 in primary hepatocytes subjected to *Hcf-1* knockdown and cultured in 25 mM glucose for 6 h in the presence of 20 μM MG132.

(G) Relative occupancy of PHF2 at the *Acc* promoter in primary hepatocytes subjected to *Hcf-1* knockdown and treated with 25 mM glucose for 4 h (n = 6 experimental repeats in hepatocytes derived from 3 mice per genotype).

(H) Relative H3K4me3 occupancy at the *Acc* promoter in primary hepatocytes subjected to *Hcf-1* knockdown and cultured in 5 or 25 mM glucose for 4 h (n = 4). Error bars are means ± SEM. *p < 0.05, **p < 0.01, ***p < 0.001; n.s., non-significant; two-way ANOVA (B–D, G, and H) or Student's t test (A, E, and F). See also Figure S7.

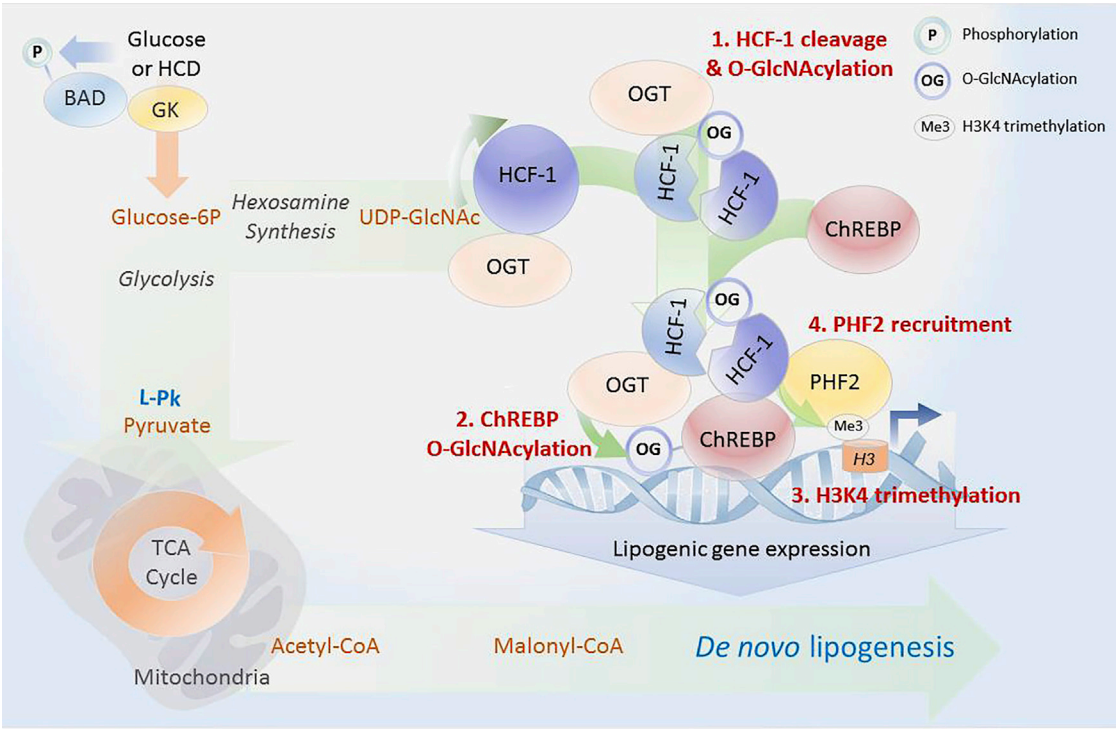

Figure 7. Proposed Biochemical Model for HCF-1 Modulation of *De Novo* Lipogenesis

Increased hepatic glucose metabolism through GK promotes DNL by providing biosynthetic precursors such as malonyl-CoA and by stimulating lipogenic gene expression via a glucose-sensitive protein complex containing HCF-1, OGT, and ChREBP. Full induction of the ChREBP transcriptional program by glucose requires HCF-1 O-GlcNAcylation (1), mediating its interaction with ChREBP, and subsequent recruitment of OGT to ChREBP (2). This augments ChREBP O-GlcNAcylation and activity. Through its association with ChREBP, HCF-1 is recruited to lipogenic gene promoters in response to glucose, where it mediates an increase in H3K4me3 histone marks (3), thereby recruiting the epigenetic activator PHF2 for enhanced transcription (4).

and HCF-1, a transcriptional co-regulator we identified as a ChREBP binding protein. Specifically, we provide multiple lines of biochemical evidence that HCF-1 O-GlcNAcylation in response to glucose or HCD first recruits OGT to ChREBP, leading to ChREBP O-GlcNAcylation and activation (Figure 7). In turn, HCF-1 is recruited to lipogenic gene promoters in a ChREBP-dependent manner, where it is required for H3K4 trimethylation and subsequent recruitment of the epigenetic activator PHF2 (Figure 7).

The discovery of HCF-1 as a regulator of ChREBP and DNL was facilitated by informative gain- and loss-of-function genetic approaches we undertook to modulate GK and the attendant glucose signals that regulate ChREBP. In addition to manipulating GK directly, we took advantage of the necessity of BAD phosphorylation for GK-mediated activation of ChREBP to effectively create a genetic system with "tuneable" glucose signaling for altering ChREBP activity. This not only provided a well-controlled platform for unbiased proteomics discovery of HCF-1 in complex with ChREBP but also enabled interrogation of the mechanisms whereby glucose regulates the assembly and function of this complex.

Numerous post-translational mechanisms modulate ChREBP activity in response to lipogenic signals (Abdul-Wahed et al., 2017; Agius, 2016a). Among these, O-GlcNAcylation regulates ChREBP DNA binding and transcriptional activity as well as protein stability (Guinez et al., 2011; Sakiyama et al., 2010; Yang and Qian, 2017). However, a specific mechanism for regulation of ChREBP O-GlcNAcylation has not been reported previously. Protein O-GlcNAcylation is the outcome of the net balance between OGT and O-GlcNAcase (OGA) activities, which transfer and remove the sugar modification, respectively. Remarkably, OGT and OGA are each encoded by a single gene, but the pair regulates O-GlcNAcylation of a multitude of substrates. Several scenarios have been proposed as to how a single *OGT* gene can specifically O-GlcNAcylate hundreds of substrates. These include specific subcellular localization of different OGT splice variants, the capacity of OGT tetratricopeptide repeats (TPRs) to control the access of specific substrates to the active site, differential sensitivity of OGT substrates to intracellular UDP-GlcNAc concentrations, and adaptor proteins that recruit the enzyme to distinct substrates (Yang and Qian, 2017). We provide evidence that HCF-1 is required for OGT recruitment to ChREBP. Moreover, this process is glucose dependent, as evident from loss- and gain-of-function approaches we undertook to modulate GK activity and examine its effect on ChREBP association with HCF-1 and OGT.

Although HCF-1 is primarily known as a transcriptional co-regulator rather than an adaptor for OGT, it can also recruit OGT and regulate the glycosylation of two other transcription factors, NRF1 and PGC1α (Lin et al., 2002; Ruan et al., 2012).

However, unlike the HCF-1:ChREBP complex, HCF-1 association with PGC1α and PGC1α O-GlcNAcylation is diminished in response to glucose stimulation or in the fed state (Ruan et al., 2012), indicating that additional mechanisms are at play to regulate the specificity of HCF-1 binding interactions and its effect on glycosylation of select partner proteins. Our studies have uncovered such a mechanism and demonstrate that HCF-1 O-GlcNAcylation itself, which, as we show, is triggered by glucose stimulation or HCD treatment, is selectively required for its binding to ChREBP but dispensable for its interaction with PGC1α. To our knowledge, this is also the first evidence assigning a specific biochemical function to HCF-1 O-GlcNAcylation. Moreover, the observation that GlcNAc or GlcN supplementation is sufficient to restore HCF-1 O-GlcNAcylation, HCF-1:ChREBP complex formation, and ChREBP O-GlcNAcylation under conditions where HBP pathway activity is decreased without global diminution in protein O-GlcNAcylation suggests that the HCF-1-ChREBP biochemical axis may be particularly sensitive to fluctuations in UDP-GlcNAc levels. Therefore, lipogenic signals may be required to secure a sufficient pool of UDP-GlcNAc for HCF-1 glycosylation and its regulated binding to ChREBP. From a conceptual standpoint, this mode of regulation is intriguing because it provides an explanation for regulated enrichment of the HCF:ChREBP complex in response to lipogenic signals.

Our findings also point to more complex effects of HCF-1 on lipogenic gene expression beyond regulation of ChREBP glycosylation. These include HCF-1-dependent H3K4 trimethylation and recruitment of the epigenetic activator PHF2 to these promoters in a glucose-dependent manner. Although PHF2 has been shown recently to be required for transcriptional activation of ChREBP target promoters (Bricambert et al., 2018), a specific mechanism for its binding to ChREBP or recruitment to these promoters was not known. As such, our finding that HCF-1 is required for PHF2 recruitment to ChREBP target promoters in response to glucose stimulation adds significant new molecular details regarding nutrient regulation of epigenetic events at ChREBP target promoters. As a transcriptional co-regulator, HCF-1 can modulate the activity of epigenetic modifiers such as histone methyl transferases (Deplus et al., 2013; Tyagi et al., 2007; Wysocka et al., 2003; Zhou et al., 2013). Although our *Hcf-1* knockdown experiments clearly show its requirement for H3K4 trimethylation in response to glucose stimulation, the identity of the specific histone methyl transferase in charge of this modification at the lipogenic gene promoters awaits further studies. Regardless, our findings indicate that ChREBP and PHF2 are part of a larger nutrient-sensitive promoter complex that contains HCF-1 as a key co-regulator and prerequisite for upregulation of activating histone marks at ChREBP target promoters.

The role of HCF-1 in hepatic metabolism is not fully understood and is likely to be context dependent. Its capacity to interact with and regulate PGC1α, a chief transcriptional regulator of fatty acid oxidation and gluconeogenesis, would be consistent with its involvement in hepatic fasting responses such as increased glucose production (Lin et al., 2002; Ruan et al., 2012). On the other hand, we show that HCF-1 is also required for transcriptional regulation of DNL through its binding and regulation of ChREBP in response to glucose stimulation or carbohydrate feeding. In this context, nutrient-induced HCF-1 O-GlcNAcylation as a specific determinant of its binding to ChREBP but not PGC1α is an attractive mechanism that could underlie the toggling of HCF-1's transcriptional regulatory roles between these two distinct nutritional states. The capacity to regulate both fatty acid oxidation and synthesis argues for a potentially broader role of HCF-1 in hepatic substrate metabolism and warrants future investigation of its significance in systemic physiology and in NAFLD.

STAR★METHODS

Detailed methods are provided in the online version of this paper and include the following:

- KEY RESOURCES TABLE
- CONTACT FOR REAGENT AND RESOURCE SHARING
- EXPERIMENTAL MODEL AND SUBJECT DETAILS
  - Mice
  - Human Liver Tissue
  - Hepatocyte Isolation and Culture Conditions
- METHOD DETAILS
  - Adenovirus Production and Viral Transduction
  - Primary Hepatocyte siRNA Transfection
  - *De Novo* Lipogenesis Assay
  - RNA Preparation and Quantitative Real-Time PCR
  - Dual Luciferase Assay
  - Chromatin Immunoprecipitation
  - Co-Immunoprecipitation and Western Blotting
  - Wheat Germ Agglutinin (WGA) Pull Down
  - *In Vitro* Cleavage and O-GlcNAcylation of HCF-1 and Pull Down Assays
  - Expression of OGT WT and D554N for HCF-1 Interaction Studies in HEK293T Cells
  - Hexosamine Pathway Metabolite Measurement
  - Nuclear Flag-ChREBP IP and LC-MS Analysis
- QUANTIFICATION AND STATISTICAL ANALYSIS

SUPPLEMENTAL INFORMATION

Supplemental Information can be found online at https://doi.org/10.1016/j.molcel.2019.05.019.

ACKNOWLEDGMENTS

We thank the Taplin Mass Spectrometry Facility at Harvard Medical School under the direction of Ross Tomaino and Steven Gygi for proteomic analysis of FLAG-ChREBP IPs; Daina Avizonis and Gaëlle Bridon for metabolite measurements at the Rosalind and Morris Goodman Cancer Research Centre Metabolomics Core Facility, supported by the Canada Foundation for Innovation, the Dr. John R. and Clara M. Fraser Memorial Trust, the Terry Fox Foundation (TFF Oncometabolism Team Grant 1048 in partnership with the Foundation du Cancer du Sein du Quebec), and McGill University; the Liver Tissue Cell Distribution System, Minneapolis, Minnesota, funded by NIH contract HHSN276201200017C, for providing normal and NASH human liver samples; Mark Magnuson, Christopher Newgard, Pere Puigserver, Mark Herman, Donald Scott, and Howard Towle for reagents; and Pere Puigserver, Suzanne Gaudet, Loren Walensky, and Mark Herman for helpful discussions. E.A.L. was supported by an NIH F31 Ruth-Kirschstein predoctoral fellowship. This work

was supported by the NIH grants R01GM094263 (to S.W.) and R01DK078081 (to N.N.D.) and a Claudia Adams Barr Award in Innovative Basic Cancer Research (to N.N.D.).

AUTHOR CONTRIBUTIONS

Conceptualization, E.A.L., D.W.C., and N.N.D.; Methodology, E.A.L., D.W.C., L.G.-H., Z.G.L., S.W., and N.N.D.; Validation, E.A.L. and D.W.C.; Investigation, E.A.L., D.W.C., M.T., and L.G.-H.; Formal Analysis, E.A.L. and D.W.C.; Writing – Original Draft, E.A.L., D.W.C., and N.N.D.; Writing – Review & Editing, E.A.L., D.W.C., Z.G.L., S.W., and N.N.D.; Funding Acquisition, E.A.L., S.W., and N.N.D.

DECLARATION OF INTERESTS

The authors declare no competing interests.

Received: November 19, 2018
Revised: March 26, 2019
Accepted: May 10, 2019
Published: June 18, 2019

REFERENCES

Abdul-Wahed, A., Guilmeau, S., and Postic, C. (2017). Sweet Sixteenth for ChREBP: Established Roles and Future Goals. Cell Metab. *26*, 324–341.

Agius, L. (2016a). Dietary carbohydrate and control of hepatic gene expression: mechanistic links from ATP and phosphate ester homeostasis to the carbohydrate-response element-binding protein. Proc. Nutr. Soc. *75*, 10–18.

Agius, L. (2016b). Hormonal and Metabolite Regulation of Hepatic Glucokinase. Annu. Rev. Nutr. *36*, 389–415.

Alves-Bezerra, M., and Cohen, D.E. (2017). Triglyceride Metabolism in the Liver. Compr. Physiol. *8*, 1–8.

Arden, C., Tudhope, S.J., Petrie, J.L., Al-Oanzi, Z.H., Cullen, K.S., Lange, A.J., Towle, H.C., and Agius, L. (2012). Fructose 2,6-bisphosphate is essential for glucose-regulated gene transcription of glucose-6-phosphatase and other ChREBP target genes in hepatocytes. Biochem. J. *443*, 111–123.

Bain, J.R., Schisler, J.C., Takeuchi, K., Newgard, C.B., and Becker, T.C. (2004). An adenovirus vector for efficient RNA interference-mediated suppression of target genes in insulinoma cells and pancreatic islets of langerhans. Diabetes *53*, 2190–2194.

Benhamed, F., Denechaud, P.-D.D., Lemoine, M., Robichon, C., Moldes, M., Bertrand-Michel, J., Ratziu, V., Serfaty, L., Housset, C., Capeau, J., et al. (2012). The lipogenic transcription factor ChREBP dissociates hepatic steatosis from insulin resistance in mice and humans. J. Clin. Invest. *122*, 2176–2194.

Bricambert, J., Miranda, J., Benhamed, F., Girard, J., Postic, C., and Dentin, R. (2010). Salt-inducible kinase 2 links transcriptional coactivator p300 phosphorylation to the prevention of ChREBP-dependent hepatic steatosis in mice. J. Clin. Invest. *120*, 4316–4331.

Bricambert, J., Alves-Guerra, M.C., Esteves, P., Prip-Buus, C., Bertrand-Michel, J., Guillou, H., Chang, C.J., Vander Wal, M.N., Canonne-Hergaux, F., Mathurin, P., et al. (2018). The histone demethylase Phf2 acts as a molecular checkpoint to prevent NAFLD progression during obesity. Nat. Commun. *9*, 2092.

Capotosti, F., Guernier, S., Lammers, F., Waridel, P., Cai, Y., Jin, J., Conaway, J.W., Conaway, R.C., and Herr, W. (2011). O-GlcNAc transferase catalyzes site-specific proteolysis of HCF-1. Cell *144*, 376–388.

Danial, N.N., Gramm, C.F., Scorrano, L., Zhang, C.Y., Krauss, S., Ranger, A.M., Datta, S.R., Greenberg, M.E., Licklider, L.J., Lowell, B.B., et al. (2003). BAD and glucokinase reside in a mitochondrial complex that integrates glycolysis and apoptosis. Nature *424*, 952–956.

Danial, N.N., Walensky, L.D., Zhang, C.-Y., Choi, C.S., Fisher, J.K., Molina, A.J., Datta, S.R., Pitter, K.L., Bird, G.H., Wikstrom, J.D., et al. (2008). Dual role of proapoptotic BAD in insulin secretion and beta cell survival. Nat. Med. *14*, 144–153.

Daou, S., Mashtalir, N., Hammond-Martel, I., Pak, H., Yu, H., Sui, G., Vogel, J.L., Kristie, T.M., and Affar, B. (2011). Crosstalk between O-GlcNAcylation and proteolytic cleavage regulates the host cell factor-1 maturation pathway. Proc. Natl. Acad. Sci. USA *108*, 2747–2752.

Dentin, R., Pégorier, J.-P., Benhamed, F., Foufelle, F., Ferré, P., Fauveau, V., Magnuson, M.A., Girard, J., and Postic, C. (2004). Hepatic glucokinase is required for the synergistic action of ChREBP and SREBP-1c on glycolytic and lipogenic gene expression. J. Biol. Chem. *279*, 20314–20326.

Dentin, R., Benhamed, F., Hainault, I., Fauveau, V., Foufelle, F., Dyck, J.R., Girard, J., and Postic, C. (2006). Liver-specific inhibition of ChREBP improves hepatic steatosis and insulin resistance in ob/ob mice. Diabetes *55*, 2159–2170.

Dentin, R., Tomas-Cobos, L., Foufelle, F., Leopold, J., Girard, J., Postic, C., and Ferré, P. (2012). Glucose 6-phosphate, rather than xylulose 5-phosphate, is required for the activation of ChREBP in response to glucose in the liver. J. Hepatol. *56*, 199–209.

Deplus, R., Delatte, B., Schwinn, M.K., Defrance, M., Méndez, J., Murphy, N., Dawson, M.A., Volkmar, M., Putmans, P., Calonne, E., et al. (2013). TET2 and TET3 regulate GlcNAcylation and H3K4 methylation through OGT and SET1/COMPASS. EMBO J. *32*, 645–655.

Eng, J.K., McCormack, A.L., and Yates, J.R. (1994). An approach to correlate tandem mass spectral data of peptides with amino acid sequences in a protein database. J. Am. Soc. Mass Spectrom. *5*, 976–989.

Fan, M., Rhee, J., St-Pierre, J., Handschin, C., Puigserver, P., Lin, J., Jäeger, S., Erdjument-Bromage, H., Tempst, P., and Spiegelman, B.M. (2004). Suppression of mitochondrial respiration through recruitment of p160 myb binding protein to PGC-1alpha: modulation by p38 MAPK. Genes Dev. *18*, 278–289.

Gibson, D.G., Young, L., Chuang, R.Y., Venter, J.C., Hutchison, C.A., 3rd, and Smith, H.O. (2009). Enzymatic assembly of DNA molecules up to several hundred kilobases. Nat. Methods *6*, 343–345.

Giménez-Cassina, A., and Danial, N.N. (2015). Regulation of mitochondrial nutrient and energy metabolism by BCL-2 family proteins. Trends Endocrinol. Metab. *26*, 165–175.

Giménez-Cassina, A., Garcia-Haro, L., Choi, C.S., Osundiji, M.A., Lane, E.A., Huang, H., Yildirim, M.A., Szlyk, B., Fisher, J.K., Polak, K., et al. (2014). Regulation of hepatic energy metabolism and gluconeogenesis by BAD. Cell Metab. *19*, 272–284.

Guinez, C., Filhoulaud, G., Rayah-Benhamed, F., Marmier, S., Dubuquoy, C., Dentin, R., Moldes, M., Burnol, A.F., Yang, X., Lefebvre, T., et al. (2011). O-GlcNAcylation increases ChREBP protein content and transcriptional activity in the liver. Diabetes *60*, 1399–1413.

Han, J.W., Valdez, J.L., Ho, D.V., Lee, C.S., Kim, H.M., Wang, X., Huang, L., and Chan, J.Y. (2017). Nuclear factor-erythroid-2 related transcription factor-1 (Nrf1) is regulated by O-GlcNAc transferase. Free Radic. Biol. Med. *110*, 196–205.

Herman, M.A., Peroni, O.D., Villoria, J., Schön, M.R., Abumrad, N.A., Blüher, M., Klein, S., and Kahn, B.B. (2012). A novel ChREBP isoform in adipose tissue regulates systemic glucose metabolism. Nature *484*, 333–338.

Hurtado del Pozo, C., Vesperinas-García, G., Rubio, M.A., Corripio-Sánchez, R., Torres-García, A.J., Obregon, M.J., and Calvo, R.M. (2011). ChREBP expression in the liver, adipose tissue and differentiated preadipocytes in human obesity. Biochim. Biophys. Acta *1811*, 1194–1200.

Iizuka, K., Wu, W., Horikawa, Y., and Takeda, J. (2013). Role of glucose-6-phosphate and xylulose-5-phosphate in the regulation of glucose-stimulated gene expression in the pancreatic β cell line, INS-1E. Endocr. J. *60*, 473–482.

Janetzko, J., Trauger, S.A., Lazarus, M.B., and Walker, S. (2016). How the glycosyltransferase OGT catalyzes amide bond cleavage. Nat. Chem. Biol. *12*, 899–901.

Kabashima, T., Kawaguchi, T., Wadzinski, B.E., and Uyeda, K. (2003). Xylulose 5-phosphate mediates glucose-induced lipogenesis by xylulose 5-phosphate-activated protein phosphatase in rat liver. Proc. Natl. Acad. Sci. USA *100*, 5107–5112.

Kim, M.S., Krawczyk, S.A., Doridot, L., Fowler, A.J., Wang, J.X., Trauger, S.A., Noh, H.L., Kang, H.J., Meissen, J.K., Blatnik, M., et al. (2016). ChREBP regulates fructose-induced glucose production independently of insulin signaling. J. Clin. Invest. *126*, 4372–4386.

Kooner, J.S., Chambers, J.C., Aguilar-Salinas, C.A., Hinds, D.A., Hyde, C.L., Warnes, G.R., Gómez Pérez, F.J., Frazer, K.A., Elliott, P., Scott, J., et al. (2008). Genome-wide scan identifies variation in MLXIPL associated with plasma triglycerides. Nat. Genet. *40*, 149–151.

Lazarus, M.B., Jiang, J., Kapuria, V., Bhuiyan, T., Janetzko, J., Zandberg, W.F., Vocadlo, D.J., Herr, W., and Walker, S. (2013). HCF-1 is cleaved in the active site of O-GlcNAc transferase. Science *342*, 1235–1239.

Lin, J., Puigserver, P., Donovan, J., Tarr, P., and Spiegelman, B.M. (2002). Peroxisome proliferator-activated receptor gamma coactivator 1beta (PGC-1beta), a novel PGC-1-related transcription coactivator associated with host cell factor. J. Biol. Chem. *277*, 1645–1648.

Lou, D.Q., Tannour, M., Selig, L., Thomas, D., Kahn, A., and Vasseur-Cognet, M. (1999). Chicken ovalbumin upstream promoter-transcription factor II, a new partner of the glucose response element of the L-type pyruvate kinase gene, acts as an inhibitor of the glucose response. J. Biol. Chem. *274*, 28385–28394.

Ma, L., Robinson, L.N., and Towle, H.C. (2006). ChREBP*Mlx is the principal mediator of glucose-induced gene expression in the liver. J. Biol. Chem. *281*, 28721–28730.

Matschinsky, F.M. (2009). Assessing the potential of glucokinase activators in diabetes therapy. Nat. Rev. Drug Discov. *8*, 399–416.

Matsumoto, M., Pocai, A., Rossetti, L., Depinho, R.A., and Accili, D. (2007). Impaired regulation of hepatic glucose production in mice lacking the forkhead transcription factor Foxo1 in liver. Cell Metab. *6*, 208–216.

Mazars, R., Gonzalez-de-Peredo, A., Cayrol, C., Lavigne, A.C., Vogel, J.L., Ortega, N., Lacroix, C., Gautier, V., Huet, G., Ray, A., et al. (2010). The THAP-zinc finger protein THAP1 associates with coactivator HCF-1 and O-GlcNAc transferase: a link between DYT6 and DYT3 dystonias. J. Biol. Chem. *285*, 13364–13371.

Metukuri, M.R., Zhang, P., Basantani, M.K., Chin, C., Stamateris, R.E., Alonso, L.C., Takane, K.K., Gramignoli, R., Strom, S.C., O'Doherty, R.M., et al. (2012). ChREBP mediates glucose-stimulated pancreatic β-cell proliferation. Diabetes *61*, 2004–2015.

Nissim, I., Horyn, O., Nissim, I., Daikhin, Y., Wehrli, S.L., Yudkoff, M., and Matschinsky, F.M. (2012). Effects of a glucokinase activator on hepatic intermediary metabolism: study with 13C-isotopomer-based metabolomics. Biochem. J. *444*, 537–551.

O'Callaghan, B.L., Koo, S.H., Wu, Y., Freake, H.C., and Towle, H.C. (2001). Glucose regulation of the acetyl-CoA carboxylase promoter PI in rat hepatocytes. J. Biol. Chem. *276*, 16033–16039.

Petrie, J.L., Al-Oanzi, Z.H., Arden, C., Tudhope, S.J., Mann, J., Kieswich, J., Yaqoob, M.M., Towle, H.C., and Agius, L. (2013). Glucose induces protein targeting to glycogen in hepatocytes by fructose 2,6-bisphosphate-mediated recruitment of MondoA to the promoter. Mol. Cell. Biol. *33*, 725–738.

Postic, C., Shiota, M., Niswender, K.D., Jetton, T.L., Chen, Y., Moates, J.M., Shelton, K.D., Lindner, J., Cherrington, A.D., and Magnuson, M.A. (1999). Dual roles for glucokinase in glucose homeostasis as determined by liver and pancreatic beta cell-specific gene knock-outs using Cre recombinase. J. Biol. Chem. *274*, 305–315.

Ruan, H.B., Han, X., Li, M.D., Singh, J.P., Qian, K., Azarhoush, S., Zhao, L., Bennett, A.M., Samuel, V.T., Wu, J., et al. (2012). O-GlcNAc transferase/host cell factor C1 complex regulates gluconeogenesis by modulating PGC-1α stability. Cell Metab. *16*, 226–237.

Sakiyama, H., Fujiwara, N., Noguchi, T., Eguchi, H., Yoshihara, D., Uyeda, K., and Suzuki, K. (2010). The role of O-linked GlcNAc modification on the glucose response of ChREBP. Biochem. Biophys. Res. Commun. *402*, 784–789.

Sanders, F.W., and Griffin, J.L. (2016). De novo lipogenesis in the liver in health and disease: more than just a shunting yard for glucose. Biol. Rev. Camb. Philos. Soc. *91*, 452–468.

Shen, D.L., Gloster, T.M., Yuzwa, S.A., and Vocadlo, D.J. (2012). Insights into O-linked N-acetylglucosamine ([0-9]O-GlcNAc) processing and dynamics through kinetic analysis of O-GlcNAc transferase and O-GlcNAcase activity on protein substrates. J. Biol. Chem. *287*, 15395–15408.

Shevchenko, A., Wilm, M., Vorm, O., and Mann, M. (1996). Mass spectrometric sequencing of proteins silver-stained polyacrylamide gels. Anal. Chem. *68*, 850–858.

Softic, S., Cohen, D.E., and Kahn, C.R. (2016). Role of Dietary Fructose and Hepatic De Novo Lipogenesis in Fatty Liver Disease. Dig. Dis. Sci. *61*, 1282–1293.

Stamatikos, A.D., da Silva, R.P., Lewis, J.T., Douglas, D.N., Kneteman, N.M., Jacobs, R.L., and Paton, C.M. (2016). Tissue Specific Effects of Dietary Carbohydrates and Obesity on ChREBPα and ChREBPβ Expression. Lipids *51*, 95–104.

Szlyk, B., Braun, C.R., Ljubicic, S., Patton, E., Bird, G.H., Osundiji, M.A., Matschinsky, F.M., Walensky, L.D., and Danial, N.N. (2014). A phospho-BAD BH3 helix activates glucokinase by a mechanism distinct from that of allosteric activators. Nat. Struct. Mol. Biol. *21*, 36–42.

Taylor, R.P., Geisler, T.S., Chambers, J.H., and McClain, D.A. (2009). Up-regulation of O-GlcNAc transferase with glucose deprivation in HepG2 cells is mediated by decreased hexosamine pathway flux. J. Biol. Chem. *284*, 3425–3432.

Thomas, L.R., Foshage, A.M., Weissmiller, A.M., Popay, T.M., Grieb, B.C., Qualls, S.J., Ng, V., Carboneau, B., Lorey, S., Eischen, C.M., and Tansey, W.P. (2016). Interaction of MYC with host cell factor-1 is mediated by the evolutionarily conserved Myc box IV motif. Oncogene *35*, 3613–3618.

Tsatsos, N.G., and Towle, H.C. (2006). Glucose activation of ChREBP in hepatocytes occurs via a two-step mechanism. Biochem. Biophys. Res. Commun. *340*, 449–456.

Tyagi, S., Chabes, A.L., Wysocka, J., and Herr, W. (2007). E2F activation of S phase promoters via association with HCF-1 and the MLL family of histone H3K4 methyltransferases. Mol. Cell *27*, 107–119.

Uyeda, K., and Repa, J.J. (2006). Carbohydrate response element binding protein, ChREBP, a transcription factor coupling hepatic glucose utilization and lipid synthesis. Cell Metab. *4*, 107–110.

Velho, G., Petersen, K.F., Perseghin, G., Hwang, J.H., Rothman, D.L., Pueyo, M.E., Cline, G.W., Froguel, P., and Shulman, G.I. (1996). Impaired hepatic glycogen synthesis in glucokinase-deficient (MODY-2) subjects. J. Clin. Invest. *98*, 1755–1761.

Wang, Y., Viscarra, J., Kim, S.J., and Sul, H.S. (2015). Transcriptional regulation of hepatic lipogenesis. Nat. Rev. Mol. Cell Biol. *16*, 678–689.

Wysocka, J., Myers, M.P., Laherty, C.D., Eisenman, R.N., and Herr, W. (2003). Human Sin3 deacetylase and trithorax-related Set1/Ash2 histone H3-K4 methyltransferase are tethered together selectively by the cell-proliferation factor HCF-1. Genes Dev. *17*, 896–911.

Yang, X., and Qian, K. (2017). Protein O-GlcNAcylation: emerging mechanisms and functions. Nat. Rev. Mol. Cell Biol. *18*, 452–465.

Yang, A.Q., Li, D., Chi, L., and Ye, X.S. (2017). Validation, Identification, and Biological Consequences of the Site-specific *O*-GlcNAcylation Dynamics of Carbohydrate-responsive Element-binding Protein (ChREBP). Mol. Cell. Proteomics *16*, 1233–1243.

Yecies, J.L., Zhang, H.H., Menon, S., Liu, S., Yecies, D., Lipovsky, A.I., Gorgun, C., Kwiatkowski, D.J., Hotamisligil, G.S., Lee, C.H., and Manning, B.D. (2011). Akt stimulates hepatic SREBP1c and lipogenesis through parallel mTORC1-dependent and independent pathways. Cell Metab. *14*, 21–32.

Zhang, P., Kumar, A., Katz, L.S., Li, L., Paulynice, M., Herman, M.A., and Scott, D.K. (2015). Induction of the ChREBPβ Isoform Is Essential for Glucose-Stimulated β-Cell Proliferation. Diabetes *64*, 4158–4170.

Zhou, P., Wang, Z., Yuan, X., Zhou, C., Liu, L., Wan, X., Zhang, F., Ding, X., Wang, C., Xiong, S., et al. (2013). Mixed lineage leukemia 5 (MLL5) protein regulates cell cycle progression and E2F1-responsive gene expression via association with host cell factor-1 (HCF-1). J. Biol. Chem. *288*, 17532–17543.

STAR★METHODS

KEY RESOURCES TABLE

REAGENT or RESOURCE	SOURCE	IDENTIFIER
Antibodies		
Rabbit polyclonal anti-ChREBP	Novus Biologicals	NB400135 lots Q1-Q3; RRID:AB_10002435
Rabbit polyclonal anti-HCF-1	Bethyl laboratories	A301-400A; RRID:AB_961015
Rabbit monoclonal anti-OGT	Cell Signaling	24083; RRID:AB_2716710
Rabbit monoclonal anti-PHF2	Cell Signaling	3497S; RRID:AB_1904085
Rabbit polyclonal anti-GCK	Santa Cruz	sc7908; RRID:AB_2107620
Rabbit monoclonal anti-BAD	Abcam	ab32445; RRID:AB_725614
Rabbit polyclonal anti-phospho BAD (S155)	Cell Signaling	9297; RRID:AB_2062131
Mouse monoclonal anti-Actin	Sigma-Aldrich	A5316; RRID:AB_476743
Rabbit IgG Isotype Control	Thermo Fisher Scientific	31235; RRID:AB_243593
Mouse monoclonal anti FLAG M2- Peroxidase	Sigma-Aldrich	A8592; RRID:AB_439702
Mouse Anti-rabbit IgG (Conformation Specific)	Cell Signaling	5127S; RRID:AB_10892860
Goat anti-rabbit IgG HRP	Jackson ImmunoResearch Laboratories	111-035-003; RRID:AB_2313567
Goat anti-mouse IgG HRP	Jackson ImmunoResearch Laboratories	115-035-003; RRID:AB_10015289
Bacterial and Virus Strains		
BAD SD. Adenovirus	Giménez-Cassina et al., 2014	PMID: 24506868
BAD AAA Adenovirus	Giménez-Cassina et al., 2014	PMID: 24506868
Gk shRNA Adenovirus	Gift of Dr. Christopher Newgard (Duke University) Bain et al., 2004	PMID: 15331526
Bad shRNA Adenovirus	Giménez-Cassina et al., 2014	PMID: 24506868
Chrebp shRNA Adenovirus	Designed from sequence in Dentin et al., 2006	PMID: 16873678
Ctrl shRNA Adenovirus	Giménez-Cassina et al., 2014	PMID: 24506868
FLAG-ChREBP Adenovirus	Gift from Dr. Donald Scott (Mount Sinai) (Metukuri et al., 2012)	PMID: 22586588
Biological Samples		
Human Liver Tissues Healthy and NASH Patients	Liver Tissue Cell Distribution System, Minneapolis, Minnesota	NIH Contract # HHSN276201200017C
Chemicals, Peptides, and Recombinant Proteins		
Phosphatase Inhibitor Cocktail 2 aqueous solution	Sigma-Aldrich	P5726
Protein Phosphatase Inhibitor Cocktail 3	Sigma-Aldrich	P0044
Phosstop, Phosphatase Inhibitor	Sigma-Aldrich	4906837001
Complete, EDTA-free Protease Inhibitor Cocktail	Sigma-Aldrich	11873580001
PuGNAC	Sigma-Aldrich	A7229
Thiamet G	Sigma-Aldrich	SML 0244
Sodium Orthovanadate	Sigma-Aldrich	S6508
Western Lightning Plus-ECL	Thermo Fisher Scientific	509049325
SuperSignal West Femto	Thermo Fisher Scientific	PI34095
NuPAGE LDS Sample Buffer (4X)	Life Technologies	NP0008
FLAG Peptide	Sigma-Aldrich	F3290
UDP-GlcNAC	Sigma-Aldrich	N/A
N-Acetyl-D-glucosamine	Sigma-Aldrich	A8625-5G
Proteinase K	Life technologies	25530015
CHELEX 100 200-400 MB	Bio-Rad Laboratories	1421253
Formaldehyde (37% solution)	Santa Cruz	sc-203049

(*Continued on next page*)

Continued

REAGENT or RESOURCE	SOURCE	IDENTIFIER
Collagenase	Sigma-Aldrich	C5138
Insulin	Sigma-Aldrich	I6634
Dexamethasone	Sigma-Aldrich	D-2915
Percoll	Sigma-Aldrich	P4937
MG132	Sigma-Aldrich	C2211
BSA Fraction IV Fatty acid free	Fischer Scientific	NC9227912
Glucosamine hydrochloride	Sigma-Aldrich	G4875
Ammonium Formate	Sigma-Aldrich	17843
Acetonitrile	Sigma-Aldrich	AX0145-1
HPLC grade water	Sigma-Aldrich	WX0008
Ammonium Acetate	Sigma-Aldrich	5330040050
U14C labeled glucose	American Radiolabled Chemical	ARC-122
Critical Commercial Assays		
Dual luciferase reagent	Promega	E1910
Targefect hepatocyte	Targeting systems	HEP-01
Trizol	Life Technologies	15596026
Syber Green Master Mix	Life Technologies	N/A
Superscript III 1st Strand Synthesis	Life Technologies	18080051
Lipofectamine RNAiMax	Life Technologies	13778150
Q5 Site-Directed Mutagenesis Kit	New England Biolabs	E0554S
Gateway LR Clonase II Enzyme mix	Thermo Fischer Scientific	11791100
TnT® Coupled Wheat Germ Extract System	Promega	L4130
Deposited Data		
Unprocessed gel images presented in this manuscript	https://doi.org/10.17632/by6b3tn4g2.1	
Experimental Models: Cell Lines		
HEK293T Cells	ATCC	CRL-3216
Experimental Models: Organisms/Strains		
C57BL/6: WT		
C57BL/6-KO (BAD)	Giménez-Cassina et al., 2014	PMID: 24506868
GKlox/lox	Gift from Dr. Mark Magnuson (Vanderbilt university): Postic et al., 1999	PMID: 9867845
C57BL/6-*alb-cre* mice	Jackson Laboratory	003574
Oligonucleotides		
Ctrl siRNA: siGenome Non-targeting siRNA #1	Dharmacon	D-001210
Hcf1 siRNA-1 sense sequence: GGA GCU UAU AGU GGU GUU U	Dharmacon	N/A
Hcf1 siRNA-2 sense sequence: AGA ACA ACA UUC CGA GGU A	Dharmacon	N/A
Primers for qPCR: See Table S1 for sequence	IDT	N/A
Recombinant DNA		
L-Pk ChORE firefly luciferase reporter	Gift from Dr. Howard Towle: Lou et al., 1999	PMID: 10497199
Acc ChORE firefly luciferase reporter	Gift from Dr. Howard Towle: O'Callaghan et al., 2001	PMID: 11340083
pCMV-Green *Renilla* Luciferase control plasmid:	Thermo Fisher Scientific	PI16153
pCMV10 3X FLAG-ChREBP	Gift from Dr. Mark Herman (Duke University)	N/A
pCMV-SPORT6 HCF-1 Plasmid	Harvard PlasmID	MmCD00320375
His-OGT WT	Janetzko et al., 2016	PMID: 27618188

(*Continued on next page*)

Continued		
REAGENT or RESOURCE	SOURCE	IDENTIFIER
His-OGT D554N	Janetzko et al., 2016	PMID: 27618188
OGT WT	This Paper	N/A
OGT D554N	This Paper	N/A
PCDNA3.1 FLAG-PGC1α	Gift from Dr. Pere Puigserver: Fan et al., 2004	PMID: 14744933
pCDNA3.1	Invitrogen	V790-20
Software and Algorithms		
ImageJ	https://imagej.nih.gov/ij/	N/A
Prism	Graph Pad	N/A
SDS 2.4 (for Q-PCR)	Applied Biosystems	N/A
MassHunter Quant	Agilent Technologies	N/A
Sequest	Thermo Fischer Scientific	N/A
Other		
Serum	Gemini	100-106 lot A16E00E
High Carbohydrate Diet (70% sucrose)	Envigo	TD.150694
WGA Beads	Vector Laboratories	AL-1023
Anti-FLAG® M2 Magnetic Beads	Sigma-Aldrich	M8823
Protein G Agarose	Sigma-Aldrich Aldrich	11719416001
DynaBeads Protein A	Thermo Fisher Scientific	10001D
Amicon Ultra Centrifugal Filters	Millipore	UFC500324

CONTACT FOR REAGENT AND RESOURCE SHARING

Further information and requests for resources and reagents should be directed to and will be fulfilled by the Lead Contact, Nika N. Danial (nika_danial@dfci.harvard.edu).

EXPERIMENTAL MODEL AND SUBJECT DETAILS

Mice

Bad −/− and conditional *Gk* mice ($Gk^{lox/lox}$) have been previously described (Giménez-Cassina et al., 2014; Postic et al., 1999). Unless otherwise indicated, mice received a standard chow diet and were housed in a barrier facility with 12 hr light and dark cycles. For high carbohydrate diet experiments, mice were fasted for 24 hr and refed a high carbohydrate diet (70% sucrose) (Envigo, TD.150694) for 18 hr.

All animal procedures were approved by the Institutional Animal Care and Use Committee at the Dana-Farber Cancer Institute.

Human Liver Tissue

Frozen human liver biopsies classified as normal (n = 7) or fatty liver (NASH) (n = 7) were provided by the Liver Tissue Cell Distribution System (LTCDS, Minneapolis, Minnesota), which was funded by the National Institutes of Health Contract # HSN276201200017C (Table S3). This study used collected specimens that had been de-identified by the LTCDS and were exempted by the Dana-Farber Cancer Institute Institutional Review Board (IRB) because it was determined that the project activities do not meet the definition of human subjects research set forth at 45 CFR 46.102 (protocol # 16-324).

Hepatocyte Isolation and Culture Conditions

Primary hepatocyte isolation and cultures were carried out as previously described with a two-step digestion process (Matsumoto et al., 2007). Briefly, livers from 8-12 week old male mice were drained of blood by perfusion via vena cava with 42°C perfusion buffer (0.4 g/L KCl, 1.0 g/L Dextrose, 1.8 g/L $NaHCO_3$, 0.2 g/L EDTA) for 3 min. Connective tissue within the liver was digested by perfusion of 42°C liver digest media (0.4 g/L KCl, 1.0 g/L Dextrose, 1.8 g/L $NaHCO_3$, 0.5 g/L CaCl2, 10 g/L BSA, 30 mg/L Collagenase) for 10 min. The liver was mechanically dissociated in plating media (DMEM: 10% FBS, 2 mM Sodium Pyruvate, 2% Pen/Strep, 1 μM Dexamethasone, 0.1 μM Insulin) at 4°C, strained through 70 micron cell strainer, and hepatocytes were collected by centrifugation at 50 g for 3 min. Hepatocytes were further isolated from other cells on a percoll gradient with centrifugation at 650 RPM for 5 min. The cell pellet was washed and resuspended in plating media, and cells were plated in plating media at a density of $8x10^5$ cells/well in 6 well plates or $4x10^6$ cells/10 cm dish unless otherwise indicated and cultured with 5% CO_2 at 37°C. Cells were starved in serum-free

M199 media supplemented with 0.2% BSA (2% Pen/Strep, 2 mM Sodium pyruvate) for 12-16 hr prior to experimental treatments.

For glucosamine (GlcN) and N-acetylglucosamine (GlcNAc) treatments, primary hepatocytes were treated with 5 mM glucosamine hydrochloride (Sigma) or 20 mM N-acetylglucosamine (Sigma) in high glucose M199 serum free media at pH 7.4 for the indicated length of time.

For MG132 treatment, primary hepatocytes treated with the indicated adenoviruses and/or siRNAs were cultured in low (5 mM) or high (25 mM) glucose for 6 hr. After 3.5 hr, the cells were treated with MG132 to a final concentration of 20 μM for the remaining 2.5 hr of the 6 hr treatment.

METHOD DETAILS

Adenovirus Production and Viral Transduction

Bad shRNA, *Gk* shRNA or scrambled shRNA and recombinant GFP, BAD S155D, and BAD AAA adenoviruses were described previously (Bain et al., 2004; Giménez-Cassina et al., 2014). Adenoviruses carrying FLAG-ChREBP were a kind gift of Dr. Donald Scott (Mount Sinai) (Metukuri et al., 2012). Adenoviruses containing the *Chrebp* shRNA were created using the following sequence **:**

gatccGTGTTGGCAATGCTGACATGttcaagagaCATGTCAGCATTGCCAACAttttttgga**g** against ChREBP from (Dentin et al., 2012). The shRNAs were ligated into pSIREN-DNR-DsRed express plasmid at BamH1 and EcoRI RE sites. The construct was excised at SalI and Spe1 sites to shuttle the hU6 promoter with the *Chrebp* shRNA sequence and ligated into pAdTrack-promoterless at the SalI and EcoRV RE sites. The adenovirus was generated using pAdEasy system (Stratagene). All virus amplification, purification, titration and verification were done using the services of ViraQuest Inc.

Adenoviral transduction of hepatocyte cultures was carried out during plating at a viral dose of 3 pfu/cell for 2-4 hr followed by 2-4 hr recovery in maintenance media (DMEM: 8 mM Glucose, 1 nM Insulin, 0.1 M Dexamethasone, 2 mM Sodium Pyruvate, 2% Pen/Strep, 10% FBS) before overnight serum starvation in M199 media (0.2% BSA) unless otherwise noted. For knockdown experiments, hepatocytes were cultured for an additional 24 hr in maintenance media before serum starvation in M199 media.

For hepatic reconstitution assays, mice were injected with a viral dose of $3x10^8$ pfu/g of body weight via tail vein, and livers were harvested 1 week after injection.

Primary Hepatocyte siRNA Transfection

Reverse siRNA transfection was performed with Lipofectamine RNAi Max (Life Technologies) per manufacturer's protocol. In brief, 150 pmol of control or *Hcf.-1* RNA duplex and 15 μL Lipofectamine RNAi max were gently mixed in 1 mL Opti-MEM and incubated for 10 min at RT before adding to freshly plated hepatocytes. For experiments that combined *Hcf-1* siRNA treatment and adenoviral expression of BAD variants, cells treated with *Hcf-1* siRNA, were left to recover for 2 hr in maintenance media (DMEM: 8 mM Glucose, 1 nM Insulin, 0.1 M Dexamethasone, 2 mM Sodium Pyruvate, 2% Pen/Strep, 10% FBS) prior to infection with adenoviruses. Cells were then harvested for analysis after 30 hr.

De Novo Lipogenesis Assay

Hepatocytes were plated at 10^6 cells per well in 6 well plates. After overnight serum starvation, hepatocytes were pretreated in 0.8 mL serum free M199 media containing 5 or 25 mM glucose for 30 min and then spiked with 1 μCi of U-^{14}C-labeled glucose (American Radiolabeled Chemicals) for 4 hr. Lipids were extracted in methanol with a modified Folch method. Briefly, cells were washed with PBS and then harvested in 200 μL of 0.5% Triton in PBS, and 500 μL of 2:1 chloroform:methanol was added to 150 μL before vortexing at high speed for 20-30 s and incubating on ice for 1 hr. The remaining protein lysate was used for protein quantification and normalization. The samples were vortexed, and 125 μL of dH_2O was added before vortexing again and centrifuging for 15 min at 1000 RPM at 4°C. The bottom phase was transferred to a large 20 mL glass scintillation vial containing 3 mL of scintillation fluid. Incorporation of ^{14}C carbons into the lipid fraction was measured using a Tri-Carb 2900 TR liquid scintillation counter (Packard), and all reads were normalized to protein content.

RNA Preparation and Quantitative Real-Time PCR

mRNA was isolated from hepatocytes plated at a density of $8x10^5$ cells/well in 6 well plates using 0.5 mL of Trizol (Life Technologies) per well, and 1 μg of RNA was used to generate cDNA by the Superscript III reverse transcriptase reagents (Life Technologies). cDNA was diluted to 200 μL (1:10 dilution), and qPCR was performed using an Applied Biosystems 7900HT Fast Real-Time PCR instrument with Syber Green reagents (Life Technologies) to a final volume of 10 μL in 384 well qPCR plates with 3 μL of diluted cDNA (1.5 μL for cyclophilin D control primers) and 300 μM primers for the indicated genes. Gene expression levels were normalized to Cyclophilin D (CycD) using the $2^{-\Delta\Delta Ct}$ method and are presented as relative transcript levels. The sequence of primers is available in Table S1.

Dual Luciferase Assay

Hepatocytes were transfected with 3 μg/mL of *Acc* (O'Callaghan et al., 2001) or *L-Pk* (Lou et al., 1999) ChoRE firefly luciferase reporters (kind gift from Dr. Howard Towle) and 10 ng/mL of CMV *Renilla* luciferase control plasmids (Thermo Fisher Scientific) using the Targefect-hepatocyte (Targeting Systems) transfection reagent. Briefly, transfection complexes were formed in 1 mL serum free high glucose DMEM without antibiotics by first adding 3 μg of DNA followed by 7.5 μL of targefect reagent and 10 μL of virofect

reagent per well followed by a 20 min incubation at 37°C. The cells were washed in antibiotic free media and 1 mL of the transfection complex was added per well in 6 well plate. Hepatocytes were cultured in maintenance media without antibiotics (DMEM: 8 mM Glucose, 1 nM Insulin, 0.1 M Dexamethasone, 2 mM Sodium Pyruvate, 10% FBS) for 4 hr for recovery and then infected with 2 pfu/cell of the indicated adenoviruses for 2 hr before overnight culture in serum free (0.2% BSA) M199 media containing 5 mM glucose. Hepatocytes were then treated for an additional 20 hr in M199 media containing 5 or 25 mM glucose. ChREBP transcriptional activity was measured by performing Promega dual luciferase assay. Briefly, cells were lysed in 500 μL of 1X passive lysis buffer (Promega), and 20 μL of lysate for each condition was transferred to a 96 well white plate. The samples were analyzed using a Berthold Technologies Mithras LB 940 instrument to inject 100 μL of LAR II reagent, measure firefly luciferase activity followed by 100 μL of Stop & Glo reagent. Renilla luciferase activity for each well was then measured individually.

Chromatin Immunoprecipitation

After overnight serum starvation, primary hepatocytes were treated with 5 or 25 mM glucose for 4 hr and washed with PBS before incubation in 1% formaldehyde (in PBS) for 10 min at 37°C. Cells were washed once in 0.125 M glycine in PBS and collected in 1 mL of PBS before centrifugation at 2000 g for 5 min at 4°C. The pellet was resuspended in 500 μL of SBAR (50 mM HEPES pH 7.4, 140 mM NaCl, 1 mM EDTA, 1% Triton, 0.1% NaDOC, 0.1% SDS, 0.5 mM PMSF, Complete EDTA-free Protease Inhibitor Cocktail), and passed through an insulin syringe several times.

Cells in SBAR buffer were sonicated in a Biorupter sonicator at middle intensity 3 times for 5 min with a 30 s ON 30 s OFF cycle at 4°C. Lysates were centrifuged for 20 min and the supernatant was transferred to a new tube. DNA concentration was measured and the equivalent of 75 μg of DNA was used per ChIP in a total volume of 200 μL of SBAR (10 μL was kept for input). Samples were incubated with 1 μg of the indicated antibody at 4°C overnight, and 10 μL of dynabeads Protein A (Invitrogen) pre-blocked with salmon sperm DNA were added to the sample and rotated for 1.5 hr at 4°C. Consecutive washes were performed in the following buffers: Buffer I (1% Triton, 0.1% NaDOC, 150 mM NaCl, 10 mM Tris.Cl pH 8), Buffer II (1% NP-40, 1% NaDOC, 150 mM KCL, 10 mM TrisCl), Buffer III (0.5% Triton, 0.1% NaDOC, 500 mM NaCl, 10 mM TrisCl), Buffer IV (0.5% NP-40, 0.5% NaDOC, 250 mM LiCl, 20 mM TrisCl, 1 mM EDTA), Buffer V (0.1% NP-40, 150 mM NaCl, 20 mM TrisCl, 1 mM EDTA), and TE for 5 min each. 100 μL of 10% Chelex resin was added to all samples to recover eluates, and 5 μL of 2 mg/mL proteinase K was added to the eluates (20 mg/mL for inputs) followed by 30 min incubation at 55°C. The digestion was then stopped by boiling the samples for 10 min. qPCR was performed using 3 μL per replica for eluates and 1 μL per replica for input. A standard curve was generated using dilutions of a pooled input sample, and ChIP samples were normalized to their respective inputs. Primers used are available in Table S1.

For liver chromatin immunoprecipitation assays, approximately 80% of the liver sample was homogenized in 5 mL of SHB (15 mM HEPES pH 7.9, 15 mM KCl, 1 mM EDTA, 50 μM spermine, 50 μM spermidine, 1.9 M sucrose, 0.5 mM PMSF, Complete EDTA-free Protease Inhibitor Cocktail) using a low speed motor-driven pestle 3 times. The liver homogenate was layered on top of 7.5 mL of cold SHB in 13.5 mL Beckman Ultra-Clear tubes and centrifuged at 25,000 RPM for 1 hr at 4°C. The pellet was gently resuspended in 400 μL of SucC buffer (15 mM HEPES pH 7.9, 60 mM KCL, 15 mM NaCl, 15 μM β-ME, 0.2 mM $MgCl_2$, 0.34 M sucrose, 0.5 mM PMSF, Complete EDTA-free Protease Inhibitor Cocktail), and transferred to a new Eppendorf tube. Formaldehyde was added to a final concentration of 1%, and the tubes were incubated for 13 min at 37°C to crosslink the DNA and protein. Crosslinking was stopped by adding glycine to a final concentration of 0.125 M followed by a 5 min incubation on ice. The homogenate was transferred to a second cushion of SucC buffer with 0.9 M sucrose in a 15 mL centrifuge tube and spun at 4,000 RPM for 15 min at 4°C before resuspending the pellet in 400 μL of SBAR buffer.

Co-Immunoprecipitation and Western Blotting

For immunoprecipitation assays (IPs), cells were lysed in buffer containing (20 mM Tris/HCl pH 7.5, 137 mM NaCl, 5% glycerol, 2 mM EDTA, 2 mM Na_3VO_4, Complete EDTA-free Protease Inhibitor Cocktail, phosphatase inhibitor cocktail 3, 2 μM Thiamet-G, 10 μM PUGNAc, 1 μM TSA, 0.15% Triton X-100). Cells were mechanically disrupted by passing through an insulin syringe and rotating for 1.5 hr at 4°C, pelleted at maximum speed in a desktop centrifuge, and the supernatant was transferred to a new tube. Immunoprecipitation was carried out with 3 mg of protein lysates and 3 μg of ChREBP antibody (Novus Biologicals, lots Q1-Q3) rotating overnight at 4°C. After overnight incubation with the antibody, 50 μL of protein G agarose beads (Sigma-Aldrich) was added to each sample followed by rotation for an additional 2 hr at 4°C. The IPs were washed once in lysis buffer, and proteins were eluted in 2X LDS sample buffer (Life Technologies) with a 10 min boil.

For western blotting without immunoprecipitation, cells were lysed in RIPA buffer (10 mM Tris/HCl, 150 mM NaCl, 1% Triton X-100 [v/v], 0.5% sodium deoxycholate, 0.1% sodium dodecyl sulfate, 10 μM PUGNAc, and 2 μM Thiamet-G, and protease inhibitors; pH 7.4), and the protein amount was quantified by BCA assay. For western blots, 10-30 μg of protein lysate was loaded.

Samples were prepared for western blotting using the NuPAGE 4X sample buffer and NuPAGE gel systems (Life Technologies). Proteins were transferred onto PVDF membrane in Towbin buffer (3.03 g/L Tris Base, 7.57 g/L Glycine, 20% methanol), and blotted with the indicated antibodies. The ImageJ software was used for quantification of band intensities.

Wheat Germ Agglutinin (WGA) Pull Down

WGA pull down assays were performed as previously described (Guinez et al., 2011). In brief, primary hepatocytes subjected to the indicated genetic manipulations and cell culture conditions were treated with MG132 (20 μM) and lysed in RIPA lysis buffer

(10 mM Tris/HCl, 150 mM NaCl, 1% Triton X-100 [v/v], 0.5% sodium deoxycholate, 0.1% sodium dodecyl sulfate, 10 μM PUGNAc, 2 μM Thiamet-G, and protease inhibitors; pH 7.4) supplemented with or without 0.5 M GlcNAc for 20 min on ice. Samples were centrifuged at 16,400 RPM for 20 min, and 1.5 mg of protein lysate was incubated with 50 μL of WGA beads (VWR) for 2 hr at 4°C.

Beads were centrifuged briefly at 2,000 RPM and subsequently washed 3 times with the following buffers: I) RIPA buffer; II) 1:1 mixture of RIPA and RIPA containing 500 mM NaCl; III) TNE (10 mM Tris/HCl, 150 mM NaCl, and 1 mM EDTA; pH 7.4). Samples were boiled in 50 μL of 2X LDS sample buffer (Life Technologies) and subjected to SDS-PAGE followed by western blotting with the indicated antibodies.

In Vitro Cleavage and O-GlcNAcylation of HCF-1 and Pull Down Assays

HCF-1 was *in vitro* transcribed and translated using the S6 promoter of the pCMV-Sport6 HCF-1 plasmid and the TnT® Coupled Wheat Germ Extract System per manufacturer's instructions (Promega, L4130).

His-OGT WT or OGT D554N proteins were purified from *E. Coli* as previously described (Janetzko et al., 2016), and used to process the *in vitro* translated HCF-1. Briefly, 5 μl of the *in vitro* synthesized HCF-1 protein was incubated with 35 μl of *in vitro* cleavage and O-GlcNAcylation assay buffer (20 mM Tris/HCl pH 7.5, 120 mM NaCl, 2 mM MgCl, 2 mM UDP-GlcNAc, 1mM fresh DTT) containing 1 or 2 μg of His-OGT WT or OGT D554N for 3 hr at 37°C.

For interaction assays, endogenous ChREBP was bound to protein G agarose beads as described in the immunoprecipitation method above. 30 μl of pre-washed, ChREBP bound beads was incubated with 40 μl of the *in vitro* processed HCF-1 protein that was diluted in 110 μl of Co-IP lysis buffer (20 mM Tris/HCl pH 7.5, 137 mM NaCl, 5% glycerol, 2 mM EDTA, 2 mM Na_3VO_4, Complete EDTA-free Protease Inhibitor Cocktail, Phosphatase inhibitor cocktail 3, 2 μM Thiamet-G, 10 μM PUGNAc, 1 μM TSA, 0.15% Triton X-100). After 1 hr rotation at 4°C, the complex was washed 2 times with lysis buffer, eluted in 50 μl of 2X LDS sample buffer (Life Technologies) and boiled for 15 min for western blot analysis.

Expression of OGT WT and D554N for HCF-1 Interaction Studies in HEK293T Cells

For mammalian expression of OGT, full-length human OGT cDNA (NM_181673.2) was amplified by PCR and inserted by isothermal assembly between the BamHI and XhoI sites in plasmid pENTR1A no ccDB (w48-1) (Gibson et al., 2009). The D554N OGT mutant was generated using the Q5 site-directed mutagenesis kit according to the manufacturer's protocols (New England Biolabs). WT and D554N OGT were inserted into the pLenti PGK Neo DEST (w531-1) vector using LR Clonase II enzyme mix (Thermo Fisher Scientific). All constructs were verified by Sanger sequencing of the complete OGT insert before use. pENTR1A no ccDB (w48-1) and pLenti PGK Neo DEST (w531-1) were gifts from Drs. Eric Campeau and Paul Kaufman (Addgene plasmid # 17398 and 19067, respectively).

Transfection of 293T cells was carried out using Lipofectamine 2000™ according to the manufacturer's instructions. In brief, one day after plating 293T cells in a 10 cm dish, 4.0 μg of the DNA mixture was incubated with 13.5 μl of Lipofectamine 2000™ in 1 mL of Opti-MEM™ for 10 min at RT. Cell media was replaced with 5 mL of pre-warmed Opti-MEM™ and the DNA mixture was added. After a 5 hr incubation, cells were incubated with newly replaced DMEM media for an additional 24 hr and subjected to WGA pull down or Co-IP experiments. For ChREBP interaction studies, the DNA mixture for transfection included the following expression vectors: 1.5 μg HCF-1, 0.5 μg ChREBP, 0.5 μg pCDN3.1, and 1.5 μg OGT WT or D554N. For PGC1α interaction studies, the DNA mixture for transfection included the following expression vectors: 1.5 μg HCF-1, 1 μg PGC1α (Fan et al., 2004), and 1.5 μg OGT WT or D554N.

Hexosamine Pathway Metabolite Measurement

Primary hepatocytes infected with the indicated adenoviruses were serum starved overnight and subsequently treated with 25 mM glucose for 5 hr. For each measurement, extracts from three 10 cm dishes were used. Cells were quickly washed twice on ice with cold 150 mM ammonium formate at pH 7.4. Plates were then placed on dry ice and scraped in 230 μL of 50% MeOH/ 50% HPLC H_2O solution and transferred to a pre-chilled tube with a metal bead. Tubes were washed with an additional 150 μL of 50% MeOH/ 50% HPLC H_2O solution and vortexed for 10 s. 220 μL of ice cold acetonitrile was added and the tubes were vortexed again for an additional 10 s. Thawed samples were placed in pre-chilled bead beater racks and beaten for 2-5 min at 30 Hz. 600 μL of dichloromethane and 300 μL of ice cold H_2O were added and tubes were vortexed for 15 s prior to 10 min incubation on ice. The samples were spun down for 5 min at 4,000 RPM at 1°C and the upper aqueous phase was transferred to a new tube on ice. The samples were spun 1 min at 13,000 RPM to remove any remaining contaminants and supernatants were transferred to a new tube on dry ice. The aqueous phase was dried using a chilled speedvac and samples were stored at −80°C until ready for LC-MS/MS data collection.

For targeted analysis and semiquantitative concentration determination of the hexosamine metabolites, 5 uL of each sample was re-suspended in 50 μL of water and injected in an Agilent 6430 Triple Quadrupole (QQQ)-LC-MS/MS. Chromatography was performed using a 1290 Infinity ultra-performance LC system (Agilent Technologies) consisting of vacuum degasser, autosampler and a binary pump. The mass spectrometer was equipped with an electrospray ionization (ESI) source and samples were analyzed in negative mode. Multiple reaction monitoring (MRM) transitions were optimized on standards for each quantitated metabolite. MRM transitions and metabolite retention times are shown in Table S2. Gas temperature and flow were set at 350°C and 10 L/min respectively, nebulizer pressure was set at 50 psi and capillary voltage was set at ± 4000V.

Chromatographic separation was performed on a Unison UK-Amino column 3 μm, 2.0x150mm (Imtakt Corp) maintained at 55°C. The chromatographic gradient started at 90% mobile phase B (acetonitrile) with a 2 min hold followed with a 18 min gradient to 100%

mobile phase A (200 mM ammonium acetate in H_2O) and then held at 100% A for 10 min at a flow rate of 0.6 mL/min. This was followed by a 6 min re-equilibration at 100% mobile phase B before the next injection. Relative concentrations were determined from external calibration curves prepared in H_2O. Additional corrections for potential sample ion suppression were not made. Data were analyzed using MassHunter Quant (Agilent Technologies).

Nuclear Flag-ChREBP IP and LC-MS Analysis

Primary hepatocytes were rinsed once with cold PBS and once with cold H_2O before being scraped in 400 μL of hypotonic lysis buffer (40 mM Tris PH 7.4, 10 mM NaCl, 1 mM EDTA, 2 mM Na_3VO_4, Complete EDTA-free Protease Inhibitor Cocktail). Cells were incubated on ice for 20 min and CHAPS was added to a final concentration of 0.5%. Cells were passed up and down in an insulin syringe 4-5 times, and nuclei were pelleted by centrifugation at 1,600 g for 7 min. The nuclei were washed 3 times in hypotonic wash buffer (hypotonic lysis buffer containing 0.5% CHAPS) and resuspended in 150 μL of hypertonic lysis buffer (40 mM Tris PH 7.4, 420 mM NaCl, 1 mM EDTA, 0.5 mM DTT, 2 mM Na_3VO_4, 0.5 mM PMSF, Complete EDTA-free Protease Inhibitor Cocktail, 0.5% CHAPS) using a hand held pestle homogenizer. Nuclei were incubated on ice for an additional 30 min with periodic vortexing, spun at 10,000 g for 30 min. The nuclear fraction (supernatant) was then transferred to a new tube.

For Co-IP experiments, nuclear fractions were concentrated using Amicon Ultra centrifugal filter units with a 3K cut off, and samples were diluted such that the final buffer concentrations was the same as Co-IP lysis buffer (20 mM Tris/HCL pH 7.4, 137 mM NaCl, 5% glycerol, 2 mM EDTA, 2 mM Na_3VO_4, Complete EDTA-free Protease Inhibitor Cocktail, 0.5% CHAPS). Anti-FLAG® M2 magnetic beads (Sigma-Aldrich) were washed 3 times in Co-IP lysis buffer and the equivalent of 20 μL of initial slurry was added to 3.5 mg of nuclear lysate. Samples were rotated for 8 hr at 4°C and washed 3 times in Co-IP lysis buffer. After the 3rd wash, proteins were eluted by resuspending the beads in 50 μL of Co-IP buffer containing 15 μg of FLAG peptides followed by incubation on a vortex platform for 30 min at 4°C. The eluate was transferred to a centrifugal filter prewashed with Co-IP buffer and the elution step was repeated. Eluates were then pooled in a single tube, TCA precipitated, and submitted for proteomic analysis at the Taplin Mass Spectrometry Facility at Harvard Medical School.

For proteomics analysis, the TCA-precipitated samples were reduced in a solution of 1 mM DTT and 50 mM ammonium bicarbonate for 30 min at 60°C. The samples were then cooled to room temperature (RT) and iodacetamide was added to a concentration of 5 mM for 15 min in the dark at RT. DTT was then added to a 5 mM concentration to quench the reaction. Sequence grade trypsin was added at a concentration of 5 ng/ μL followed by overnight incubation at 37°C. The samples were then desalted by an in house-made desalting column, dried in a speed vac, and stored at 4°C until analysis.

On the day of analysis, the samples were reconstituted in 5-10 μl of HPLC solvent A (2.5% acetonitrile, 0.1% formic acid). A nano-scale reverse-phase HPLC capillary column was created by packing 2.6 μm C18 spherical silica beads into a fused silica capillary (100 μm inner diameter x ~30 cm length) with a flame-drawn tip (Shevchenko et al., 1996). After equilibrating the column, each sample was loaded via a Famos auto sampler (LC Packings) onto the column. A gradient was formed and peptides were eluted with increasing concentrations of solvent B (97.5% acetonitrile, 0.1% formic acid).

As peptides eluted they were subjected to electrospray ionization and entered into an LTQ Orbitrap Velos Pro ion-trap mass spectrometer (Thermo Fisher Scientific). Peptides were detected, isolated, and fragmented to produce a tandem mass spectrum of specific fragment ions for each peptide. Peptide sequences (and hence protein identity) were determined by matching protein databases with the acquired fragmentation pattern by the software program, Sequest (Thermo Fisher Scientific) (Eng et al., 1994). All databases include a reversed version of all the sequences and the data was filtered to between a one and two percent peptide false discovery rate (FDR).

The spectral counts for the identified proteins in Flag-ChREBP immunoprecipitates were normalized to ChREBP spectral counts in each IP sample. Proteins that were enriched 3-fold or more in WT compared to *Bad* −/− samples were prioritized for analysis using online databases, including DAVID, STRING, Panther, UniProt, and PubMed literature search. Proteins known to interact with other transcription factors were highlighted by STRING analysis. Proteins with direct or indirect functional annotations in metabolism and transcription were identified by gene ontology in DAVID and Panther, and proteins with indirect annotations in metabolism and transcription were identified by UniProt and PubMed literature searches. Proteins with exclusively mitochondrial or endoplasmic reticulum localization were excluded from the list.

QUANTIFICATION AND STATISTICAL ANALYSIS

Data are presented as mean ± SEM of the indicated number of independent hepatocyte isolations or mice per genotype in the figure legends. Statistical significance among the groups was tested with unpaired or paired Student's t test and ANOVA with Tukey's post hoc multiple comparison test when appropriate using the GraphPad Prism software. Differences were considered significant at $p < 0.05$. Unless otherwise indicated, n denotes the number of independent hepatocyte isolations or mice.

Molecular Cell, Volume *75*

Supplemental Information

HCF-1 Regulates *De Novo* Lipogenesis through a Nutrient-Sensitive Complex with ChREBP

Elizabeth A. Lane, Dong Wook Choi, Luisa Garcia-Haro, Zebulon G. Levine, Meghan Tedoldi, Suzanne Walker, and Nika N. Danial

Table S1 related to Figure 1. qPCR Primers	
Primer Name	**Sequence**
L-Pk F	ctg gaa cac ctc tgc ctt ctg
L-Pk R	cac aat ttc cac ctc cga ctc
Acc1 F	aca gtg gag cta gaa ttg gac
Acc1 R	act tcc cga cca agg act ttg
Scd1 F	ccg gag acc ctt aga tcg a
Scd1 R	tag cct gta aaa gat ttc tgc aaa cc
Elovl6 F	gaa caa gcg agc caa gtt tg
Elovl6 R	tgt aag cac cag ttc gaa gag
Fas F	agc ggc cat ttc cat tgc cc
Fas R	cca tgc cca gag ggt ggt tg
Chrebpα F	ttg ttc agc cgg atc ttg tc
Chrebpα R	agc atc gat ccg aca ctc ac
Chrebpβ F	tct gca gat cgc gtg gag
Chrebpβ R	ctt gtc ccg gca tag caa
Srebp1c F	aac gtc act tcc agc tag ac
Srebp1c R	cca cta agg tgc cta cag agc
Acly F	gaa gct gac ctt gct gaa cc
Acly R	ctg cct cca atg atg agg at
Me F	gcc ggc tct atc ctc ctt tg
Me R	ttt gta tgc atc ttg cac aat ctt t
Pdhk F	tct aac gtc gcc aga att aaa gc
Pdhk R	gga acg tac acg atg tgg att
CycD F	atg gca ctg gcg gca ggt cc
CycD R	ttg cca ttc ctg gac cca aa
L-Pk ChORE F	gtc cca cac ttt gga agc at
L-Pk ChORE R	ccc aac act gat tct acc c
Acc1 ChORE F	gag gcc agt ttc cac tga ct
Acc1 ChORE R	tgg att gcc aat gat cac t

Table S2 related to Figure 4. Retention Times and MRM Transitions for Hexosamines
(Quantifying transition is indicated in bold letters)

Metabolite	**MRM Transitions**	**Retention time (min)**	**Polarity**
N-acetyl-glucosamine-6-phosphate	**302→284** 302→168 302→126 302→108	11.0	Pos
UDP-N-acetyl-glucosamine	**608→204** 608→138	9.1	Pos

Table S3 related to Figure 6. List of Human Liver Specimens				
Sample ID	Diagnoses	Sex	Age	COD
HH 1142	Normal	M	19	HT/MVA
HH 1170	Normal	F	49	ICH
HH 1174	Normal	F	72	ICH
HH 1202	Normal	F	67	CVA
HH 1211	Normal	M	79	Anoxia
HH 1227	Normal	M	34	CVA
HH 1249	Normal	M	59	CVA
UMN 1098	NASH-Fatty	F	59	N/A
UMN 1152	NASH-Fatty	F	41	N/A
UMN 1228	NASH-Fatty	M	62	N/A
UMN 1242	NASH-Fatty	F	43	N/A
UMN 1249	NASH-Fatty	F	55	N/A
UMN 1305	NASH-Fatty	F	48	N/A
UMN 1370	NASH-Fatty	M	53	N/A

COD: Cause of death; HT/MVA: Head trauma/ motor vehicle accident; ICH: Intracerebral hemorrhage; CVA: Cerebrovascular accident.

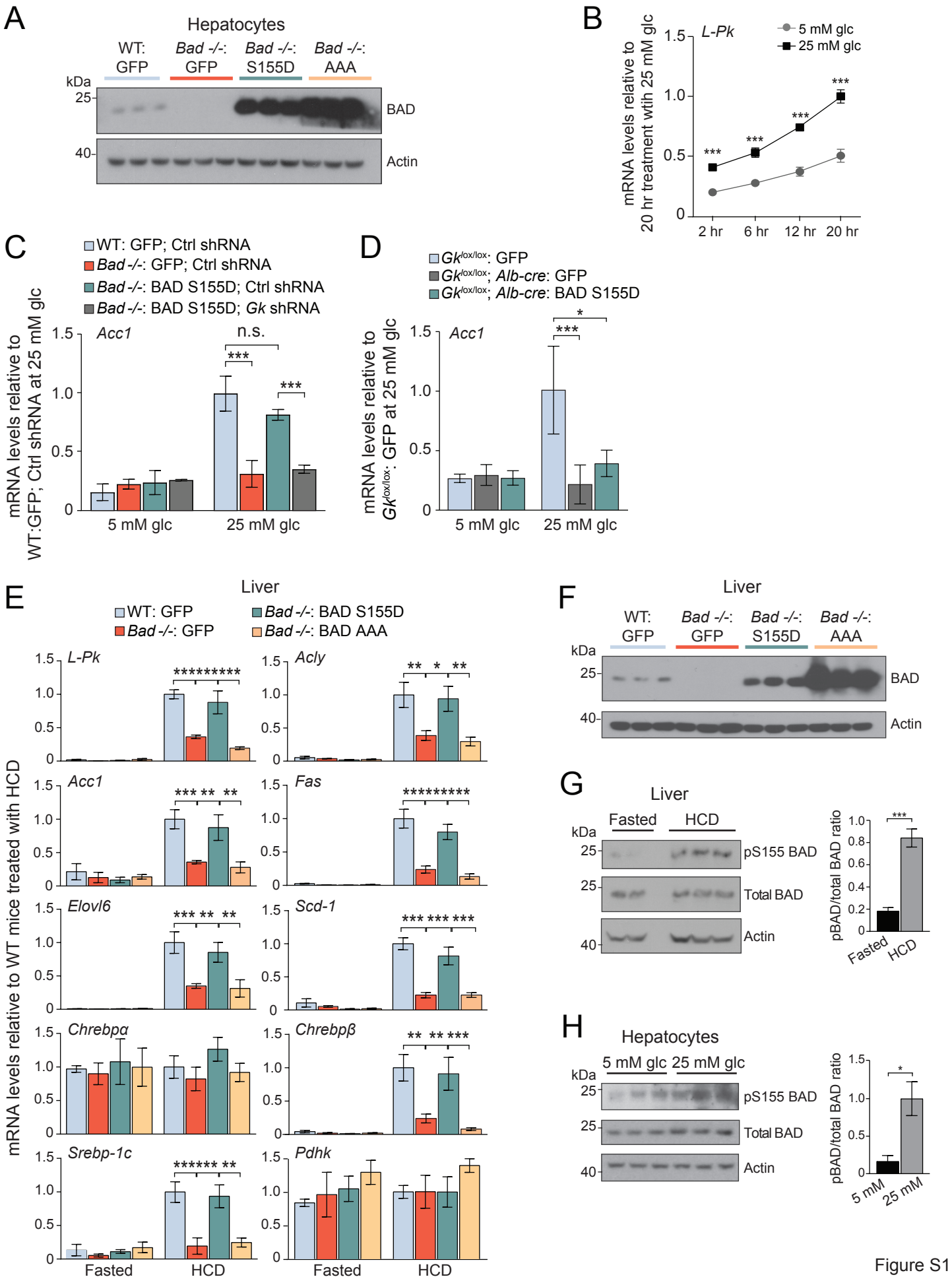
A
Hepatocytes
WT: GFP
Bad -/-: GFP
Bad -/-: S155D
Bad -/-: AAA
kDa
25
40
BAD
Actin
B
L-Pk
5 mM glc
25 mM glc
mRNA levels relative to 20 hr treatment wtih 25 mM glc
2 hr
6 hr
12 hr
20 hr
C
WT: GFP; Ctrl shRNA
Bad -/-: GFP; Ctrl shRNA
Bad -/-: BAD S155D; Ctrl shRNA
Bad -/-: BAD S155D; Gk shRNA
Acc1
n.s.
mRNA levels relative to WT:GFP; Ctrl shRNA at 25 mM glc
5 mM glc
25 mM glc
D
Gklox/lox: GFP
Gklox/lox; Alb-cre: GFP
Gklox/lox; Alb-cre: BAD S155D
Acc1
mRNA levels relative to Gklox/lox: GFP at 25 mM glc
5 mM glc
25 mM glc
E
Liver
WT: GFP
Bad -/-: GFP
Bad -/-: BAD S155D
Bad -/-: BAD AAA
L-Pk
Acly
Acc1
Fas
Elovl6
Scd-1
Chrebpα
Chrebpβ
Srebp-1c
Pdhk
mRNA levels relative to WT mice treated with HCD
Fasted
HCD
F
Liver
WT: GFP
Bad -/-: GFP
Bad -/-: S155D
Bad -/-: AAA
kDa
25
40
BAD
Actin
G
Liver
Fasted
HCD
kDa
25
25
40
pS155 BAD
Total BAD
Actin
pBAD/total BAD ratio
Fasted
HCD
H
Hepatocytes
5 mM glc
25 mM glc
kDa
25
25
40
pS155 BAD
Total BAD
Actin
pBAD/total BAD ratio
5 mM
25 mM

Figure S1

Figure S1, related to Figure 1. The effect of BAD modifications on *de novo* lipogenesis

(A) BAD protein levels in WT and *Bad -/-* primary hepatocytes after reconstitution with the indicated adenoviruses.

(B) Time course of changes in *L-Pk* transcription in WT primary hepatocytes treated with 5 or 25 mM glucose (n=4 experimental repeats in hepatocytes derived from 2 mice per genotype). For all subsequent gene expression analyses, glucose treatment was carried out for 20 hrs.

(C) Relative expression of *Acc1* mRNA in WT and *Bad -/-* primary hepatocytes infected with the indicated adenoviruses and treated with 5 or 25 mM glucose for 20 hrs (n=2-3 experimental repeats in hepatocytes derived from one mouse per genotype).

(D) Relative expression of *Acc1* mRNA in hepatocytes derived from control ($Gk^{lox/lox}$) or liver-specific GK-deficient mice ($Gk^{lox/lox}$; *Alb-cre*) infected with the indicated adenoviruses and treated with 5 or 25 mM glucose for 20 hrs (n=4-6 experimental repeats in hepatocytes derived from 2 mice per genotype).

(E-F) Relative expression of hepatic lipogenic genes in livers of WT and *Bad -/-* mice reconstituted with the indicated adenoviruses one week prior to being fasted for 24 hrs and refed a HCD for 18 hrs (E), (n=3-4). Western blots in (F) show BAD protein levels in liver samples used in (E).

(G) Immunoblot analysis and quantification of relative BAD phosphorylation on S155 in liver samples from C57BL/6J mice fasted for 24hrs or fasted then refed a HCD for 18hrs (n=2-3).

(H) Immunoblot analysis and quantification of relative BAD phosphorylation on S155 in primary hepatocytes from C57BL/6J mice cultured in 5 or 25 mM glucose for 4 hrs (n=3).

Error bars are means ± SD (B-D) or ± SEM (E,G-H), *$p < 0.05$; **$p < 0.01$; ***$p < 0.001$; n.s., non-significant; two way ANOVA (B-E) or Student's t test (G-H).

A

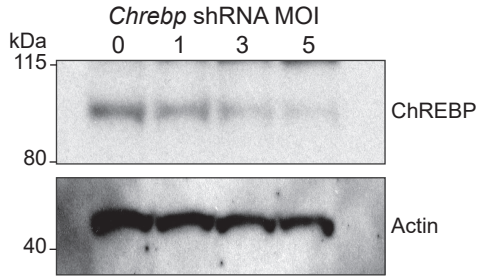
Chrebp shRNA MOI
kDa
0
1
3
5
115
80
40
ChREBP
Actin

B

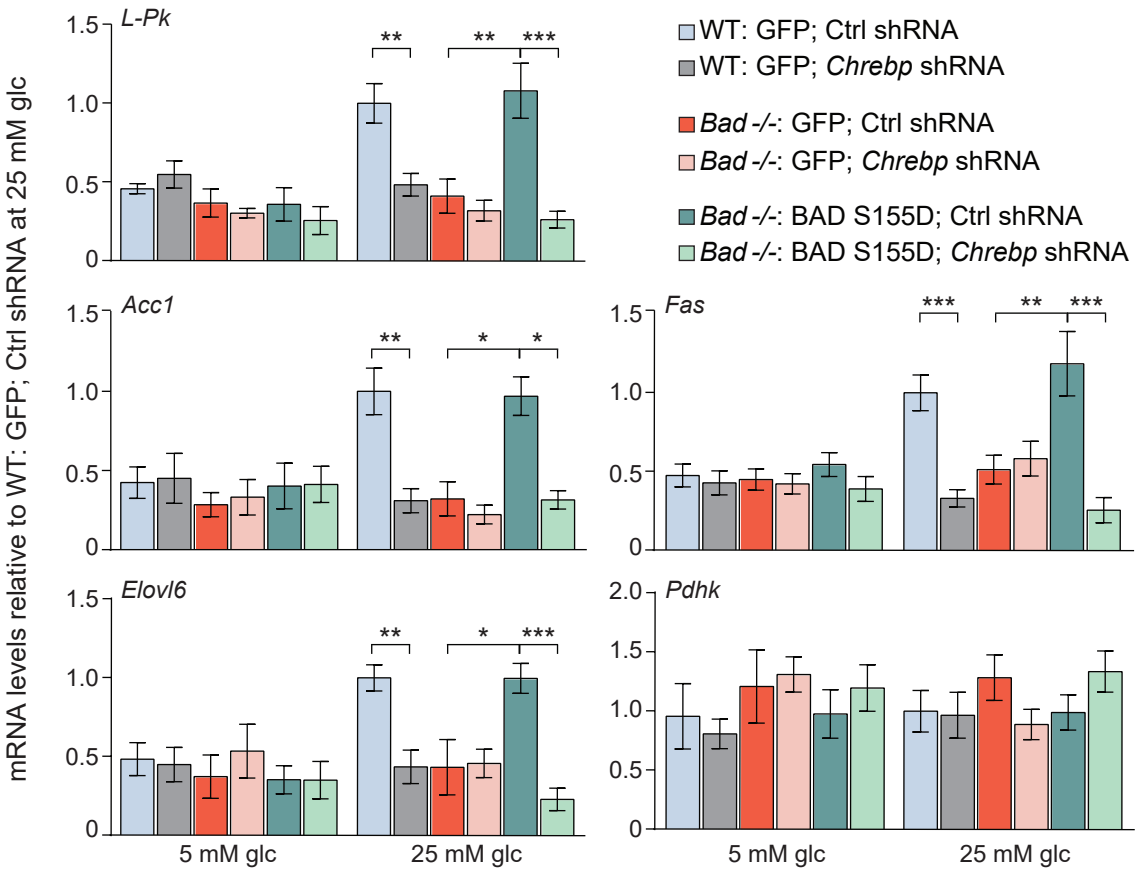
mRNA levels relative to WT: GFP; Ctrl shRNA at 25 mM glc
L-Pk
Acc1
Fas
Elovl6
Pdhk
WT: GFP; Ctrl shRNA
WT: GFP; Chrebp shRNA
Bad -/-: GFP; Ctrl shRNA
Bad -/-: GFP; Chrebp shRNA
Bad -/-: BAD S155D; Ctrl shRNA
Bad -/-: BAD S155D; Chrebp shRNA
5 mM glc
25 mM glc

Figure S2

Figure S2, related to Figure 1. The effect of BAD modifications on ChREBP-dependent *de novo* lipogenesis

(A) Efficiency of *ChREBP* shRNA-expressing adenovirus to deplete ChREBP protein levels in WT primary hepatocytes. MOI; multiplicity of infection

(B) Relative mRNA abundance of lipogenic genes in WT and *Bad* -/- primary hepatocytes co-infected with the indicated adenoviruses and treated with 5 or 25 mM glucose for 20 hrs (n=4).

Error bars in B are means ± SEM, *p < 0.05; **p < 0.01; ***p < 0.001; two way ANOVA.

A

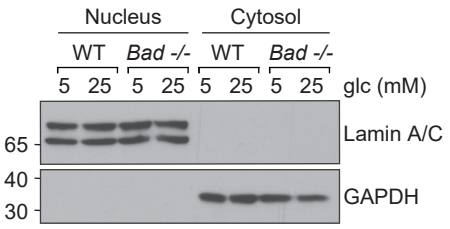

B

Gene Name	Unique Peptides		Total Peptides		Corrected Ratio WT to *Bad-/-*	Peptide sequences (WT)
	WT	*Bad -/-*	WT	*Bad -/-*		
ChREBP	26	26	32	37	1	See panel S2C below
Mlx	6	5	6	6	1.6	R.RGAPQLSPESPLLSGAR.G = 38-56 R.GAPQLSPESPLLSGAR.G = 39-56 K.VEYAYSDNSLDPGLFVESTHK.G = 68-90 K.KKQEEEVSTLR.K = 191-203 K.VNYEQIVK.A = 212-221 K.AHQDNPHEGEDQVSDQVK.F = 220-239
HCF-1	9	3	9	3	3.5	R.LLVFGGM*VEYGK.Y = 93-106 R.LGHSFSLVGNK.C = 137-148 K.VASSPVM*VSNPATR.M = 594-609 K.VMTSGTGAPAK.I = 802-814 K.IATGHGQQGVTQVVLK.G = 820-837 K.GAPGQPGTILR.T = 836-844 R.TTNTPTVVR.I = 1137-1147 K.KQELQPGTAYK.F = 1862-1874 R.GPFSEISAFK.T = 1884-1895

C

ChREBP Protein coverage in WT FLAG IP

MARALADLSV NLQVPR**VVPS PDSDSDTDLE DPSPR**RSAGG LHR**SQVIHSG HF MVSSPHSD SLTRRRDQEG PVGLADFGPR** SIDPTLTHLF ECLSLAYSGK LVSPK WKNFK GLKLLCRDKI R**LNNAIWRAW YIQYVQR**RKS PVCGFVTPLQ GSEADEH R**KP EAVILEGNYW KRRIEVVMR**E YHKWRIYYKK RLRKSSREGD FLAPK**QVEG G WPPPER**WCEQ LFSSVVPVLL GGSEEEPGGR QLLDLDCFLS DISDTLFTMT Q PSPSSLQLP PEDAYVGNAD MIQPDLTPLQ PSLDDFMEIS DFFTNYRPPQ TPTS SNYIES PSFGPMADSL FSSGILAPEM PSPASSSSSS GMTPHSGNTR LQARNS CSGP LDPNPFLSSE FLLPEDPKTK IPPAPGPTPL LPFPTPVKVH GLEPCTPSPF PTMAPPPSLL PEESLLSARF PFTSAPPAPG VSTLPAPTTF VPTPQPGPGP VPF SVDHLPH GYLEPVFGPH FTVPQGMQPR CKPSSPSPGG QK**ASPPTLAS ATAS PTATAT AR**DNNPCLTQ LLR**AAKPEQA LEPPTMPGTL LRPPESPQDT VSEIPR**A RAF FPPIPAPTPP RPPPGPATLA PPRSLVVPKA ER**LSPPASSG SERR LSGDLN SIQPSGALSV HLSPPQTVLS R**GRVDNNKME NRR**RITHISAE QK**RRFNIKLG FDT LHGLVST LSAQPSLK**VS KATTLQK**TAE YILMLQQERA AMQEEAQQLR** DEIEEL NAAI NLCQQQLPAT GVPITHQR**FD QMRDMFDDYV R**TRTLHNWKF WVFSILIRP L FESFNGMVST ASLHSLRQTS LAWLEQYCSL PALRPTVLNS LR**QLSTSTSI LTD PSLVPEQ ATRAVTEGTL GRPL**

ChREBP Protein coverage in *Bad -/-* FLAG IP

MARALADLSV NLQVPR**VVPS PDSDSDTDLE DPSPR**RSAGG LHR**SQVIHSG HF MVSSPHSD SLTRRRDQEG PVGLADFGPR** SIDPTLTHLF ECLSLAYSGK LVSPK WKNFK GLKLLCRDKI R**LNNAIWRAW YIQYVQR**RKS PVCGFVTPLQ GSEADEH R**KP EAVILEGNYW KRRIEVVMR**E YHKWRIYYKK RLRKSSREGD FLAPK**QVEG G WPPPER**WCEQ LFSSVVPVLL GGSEEEPGGR QLLDLDCFLS DISDTLFTMTQ PSPSSLQLP PEDAYVGNAD MIQPDLTPLQ PSLDDFMEIS DFFTNYRPPQ TPTS SNYIES PSFGPMADSL FSSGILAPEM PSPASSSSSS GMTPHSGNTR LQARNS CSGP LDPNPFLSSE FLLPEDPKTK IPPAPGPTPL LPFPTPVKVH GLEPCTPSPF PTMAPPPSLL PEESLLSARF PFTSAPPAPG VSTLPAPTTF VPTPQPGPGP VPF SVDHLPH GYLEPVFGPH FTVPQGMQPR CKPSSPSPGG QK**ASPPTLAS ATAS PTATAT AR**DNNPCLTQ LLR**AAKPEQA LEPPTMPGTL LRPPESPQDT VSEIPR**A RAF FPPIPAPTPP RPPPGPATLA PPRSLVVPKA ER**LSPPASSG SERR LSGDLN SIQPSGALSV HLSPPQTVLS R**GRVDNNKME NRR**ITHISAE QK**RRFNIKLG FDT LHGLVST LSAQPSLKVS KATTLQK**TAE YILMLQQERA AMQEEAQQLR** DEIEEL NAAI NLCQQQLPAT GVPITHQR**FD QMRDMFDDYV R**TRTLHNWKF WVFSILIRP L FESFNGMVST ASLHSLRQTS LAWLEQYCSL PALRPTVLNS LR**QLSTSTSI LTD PSLVPEQ ATRAVTEGTL GRPL**

D

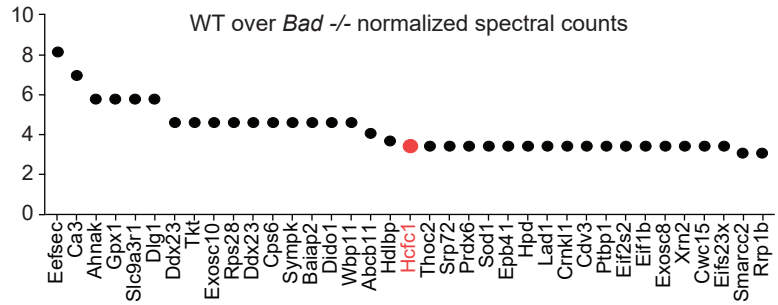

E

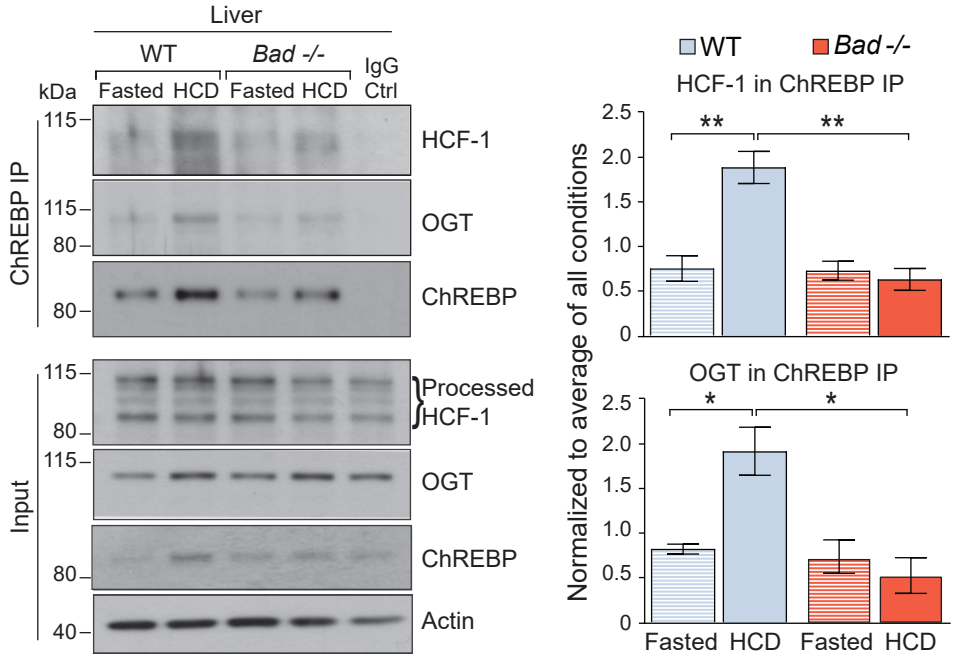

Figure S3

Figure S3, related to Figure 2. Identification of HCF-1 as a previously unknown ChREBP-interacting protein

(A) Purity of nuclear fractions generated for Flag-ChREBP protein interactome studies as determined by western blot analyses using antibodies to Lamin A/C and GAPDH as nuclear and cytosolic markers, respectively. Nuclear fractions from WT and *Bad* -/- hepatocytes treated with 25 mM glucose were subsequently used for immunoprecipitation and mass spectrometry analyses.

(B) Summary of mass spectrometry (MS) results for ChREBP, Mlx and HCF-1 in anti-Flag immunoprecipitates of nuclear fractions from Flag-ChREBP-expressing WT and *Bad* -/- hepatocytes treated with 25 mM glucose for 6 hrs. Corrected ratios were calculated by normalizing total peptide spectral counts for each protein to the total peptide spectral counts for ChREBP in each genotype. Corresponding amino acid residues for each peptide in the mouse Mlx or HCF-1 are indicated.

(C) Protein coverage of ChREBP in MS experiment in (B). Sequences underlined in green are peptides captured in the proteomics data set.

(D) Proteins enriched by 3 fold or more in ChREBP immunoprecipitates from nuclear fractions of WT versus *Bad* -/- primary hepatocytes treated as in A.

(E) Representative western blots (left) and quantification of n=3 experiments (right) of ChREBP association with HCF-1 and OGT in livers derived from WT and *Bad* -/- mice fasted for 24 hrs and refed with a HCD for 18 hrs.

Error bars in E are means ± SEM, *$p < 0.05$; **$p < 0.01$; two way ANOVA.

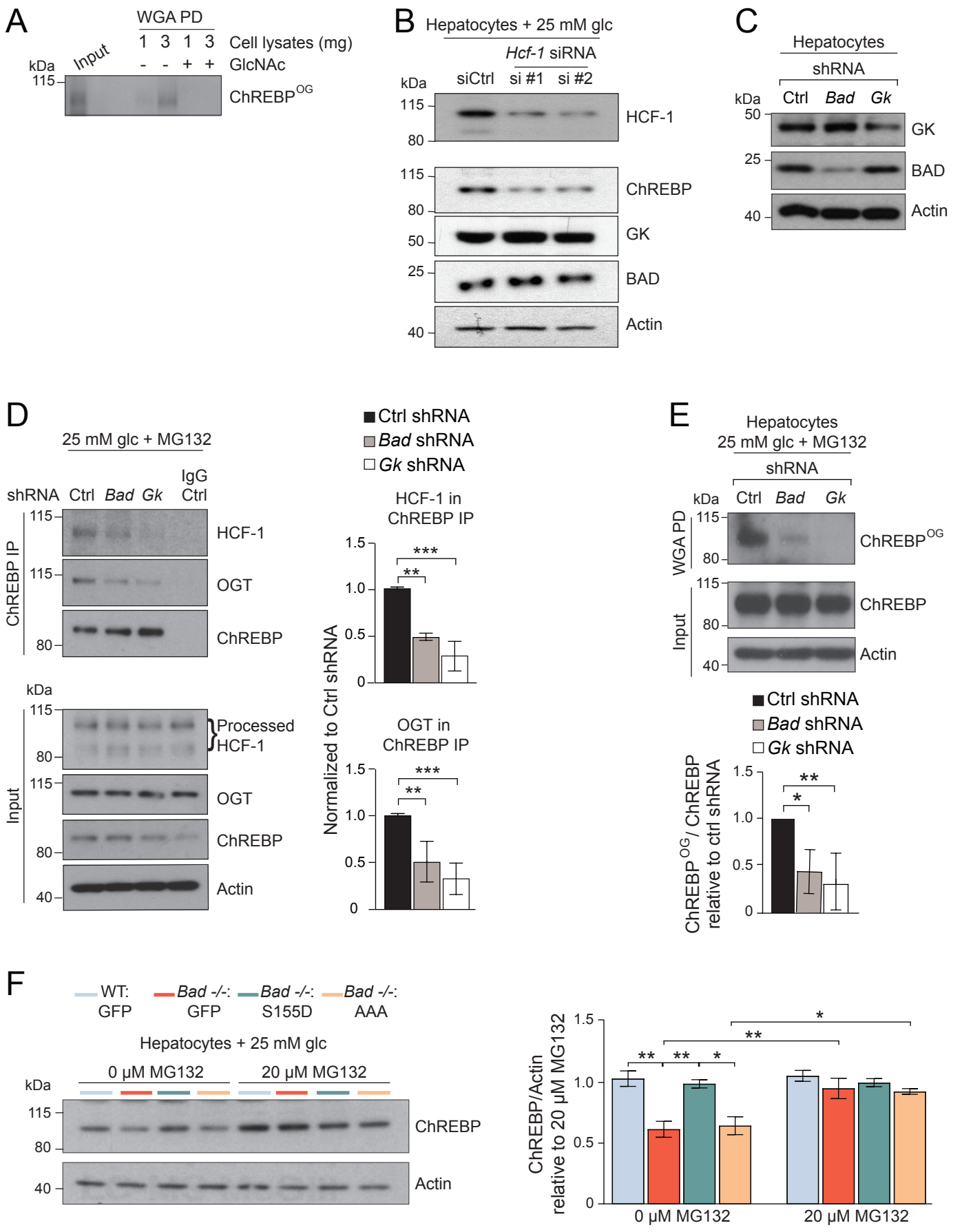
A
WGA PD
1 3 1 3
Cell lysates (mg)
- - + + GlcNAc
kDa
Input
115
ChREBP^OG
B
Hepatocytes + 25 mM glc
Hcf-1 siRNA
siCtrl si #1 si #2
kDa
115
80
HCF-1
115
80
ChREBP
50
GK
25
BAD
40
Actin
C
Hepatocytes
shRNA
kDa
Ctrl Bad Gk
50
GK
25
BAD
40
Actin
D
25 mM glc + MG132
shRNA Ctrl Bad Gk
IgG Ctrl
ChREBP IP
115
HCF-1
115
OGT
80
ChREBP
kDa
115
Processed HCF-1
80
Input
115
OGT
80
ChREBP
40
Actin
Ctrl shRNA
Bad shRNA
Gk shRNA
HCF-1 in ChREBP IP
Normalized to Ctrl shRNA
1.5
1.0
0.5
0
***
**
OGT in ChREBP IP
1.5
1.0
0.5
0
***
**
E
Hepatocytes
25 mM glc + MG132
shRNA
kDa
Ctrl Bad Gk
WGA PD
115
80
ChREBP^OG
Input
115
80
ChREBP
40
Actin
Ctrl shRNA
Bad shRNA
Gk shRNA
ChREBP^OG / ChREBP relative to ctrl shRNA
1.5
1.0
0.5
0
**
*
F
WT: GFP
Bad -/-: GFP
Bad -/-: S155D
Bad -/-: AAA
Hepatocytes + 25 mM glc
0 μM MG132
20 μM MG132
kDa
115
80
ChREBP
40
Actin
ChREBP/Actin relative to 20 μM MG132
1.5
1.0
0.5
0
**
**
*
*
**
0 μM MG132
20 μM MG132

Figure S4

Figure S4, related to Figure 2. Identification of HCF-1 as a previously unknown ChREBP-interacting protein

(A) Validation of WGA pull down assay for the capture of O-GlcNAcylated ChREBP. O-GlcNAcylated ChREBP capture is competed off by GlcNAc treatment.

(B) ChREBP protein levels in WT hepatocytes treated with two independent *Hcf-1* siRNAs in the presence of 25 mM glucose.

(C) BAD and GK protein levels in primary hepatocytes subjected to shRNA-mediated knockdown of *Bad* or *Gk*.

(D) Representative western blots (left) and quantification of n=3 experiments (right) of ChREBP association with HCF-1 and OGT in WT primary hepatocytes subjected to *Bad* or *Gk* knockdown as in (C), and cultured in 25 mM glucose for 6 hrs in the presence of 20 μM MG132.

(E) Representative western blots (top) and quantification of n=3 experiments (bottom) of $ChREBP^{OG}$ in WGA pull down assays in WT primary hepatocytes subjected to *Bad* or *Gk* knockdown as in (C), and cultured in 25 mM glucose for 6 hrs in the presence of 20 μM MG132.

(F) Representative western blots (left) and quantification of n=3 experiments (right) of ChREBP protein levels in primary WT and *Bad* -/- hepatocytes reconstituted with the indicated BAD mutants and cultured in 25 mM glucose for 6 hrs in the presence or absence of 20 μm MG132.

Error bars in D-F are means ± SEM, *$p < 0.05$; **$p < 0.01$; ***$p < 0.001$; one way ANOVA (D-E) or two way ANOVA (F).

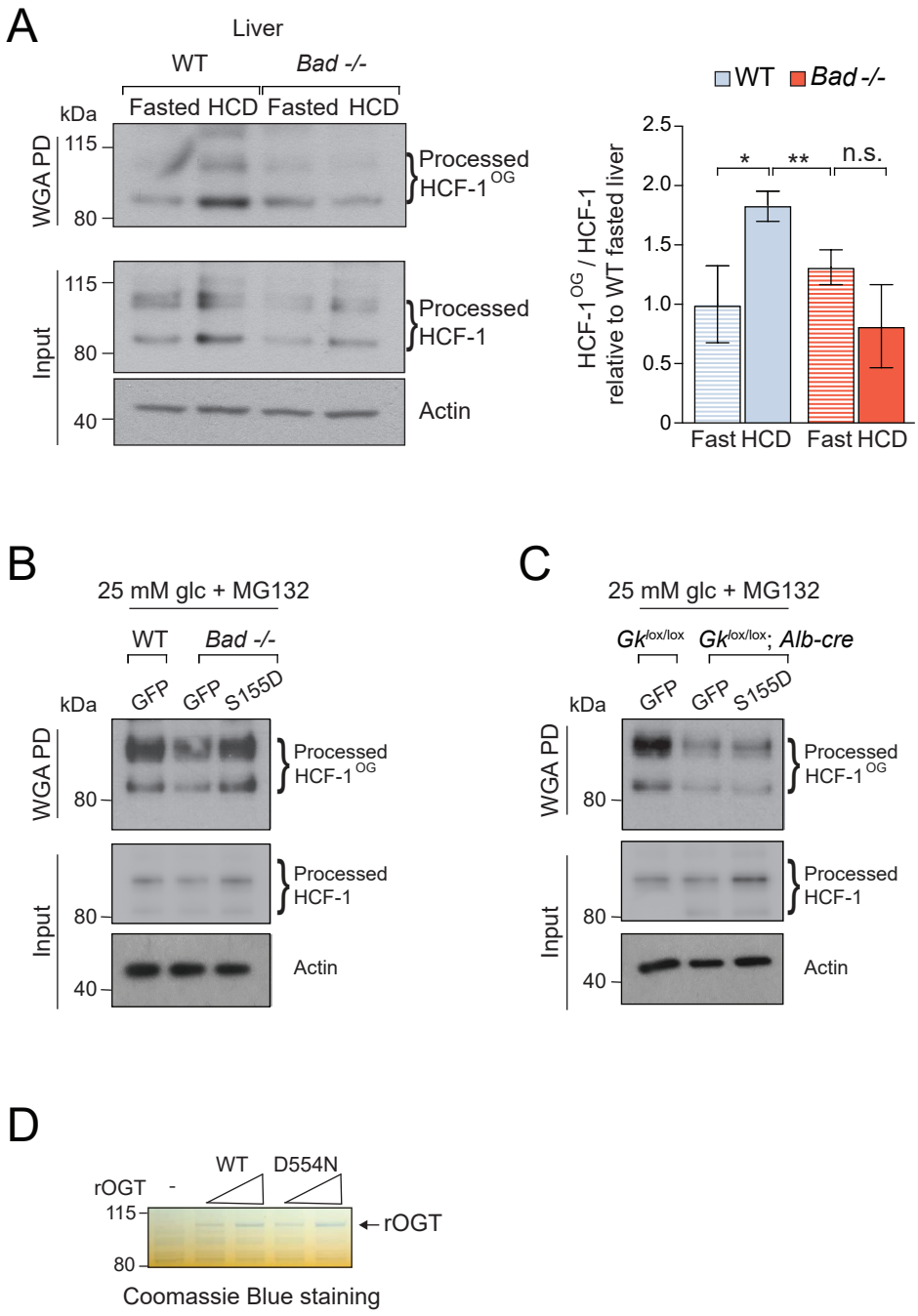
A
Liver
WT
Bad -/-
Fasted HCD Fasted HCD
kDa
WGA PD
115
80
Processed HCF-1 OG
Input
115
80
Processed HCF-1
40
Actin
WT Bad -/-
HCF-1 OG / HCF-1 relative to WT fasted liver
2.5
2.0
1.5
1.0
0.5
0
*
**
n.s.
Fast HCD Fast HCD
B
25 mM glc + MG132
WT
Bad -/-
GFP GFP S155D
kDa
WGA PD
80
Processed HCF-1 OG
Input
80
Processed HCF-1
40
Actin
C
25 mM glc + MG132
Gk lox/lox
Gk lox/lox; Alb-cre
GFP GFP S155D
kDa
WGA PD
80
Processed HCF-1 OG
Input
80
Processed HCF-1
40
Actin
D
WT D554N
rOGT -
115
80
rOGT
Coomassie Blue staining

Figure S5

Figure S5, related to Figure 3. HCF-1 O-GlcNAcylation is induced by lipogenic signals and is required for its interaction with ChREBP.

(A) Representative western blots (left) and quantification of n=3 experiments (right) of HCF-1^{OG} in livers from WT and *Bad -/-* mice fasted for 24 hrs and refed a HCD for 18 hrs.

(B) Analysis of HCF-1 O-GlcNAcylation by WGA pull down in WT and *Bad -/-* primary hepatocytes infected with the indicated adenoviruses and cultured in 25 mM glucose for 6 hrs in the presence of 20 μM MG132.

(C) Analysis of HCF-1 O-GlcNAcylation by WGA pull down in hepatocytes derived from control ($Gk^{lox/lox}$) or liver-specific GK-deficient mice ($Gk^{lox/lox}$; *Alb-cre*) that were infected with the indicated adenoviruses and cultured as in (B).

(D) Recombinant WT or D554N OGT (rOGT) used in Figure 3D.

Error bars in A are means ± SEM, *p < 0.05; **p < 0.01; n.s., non-significant; two way ANOVA.

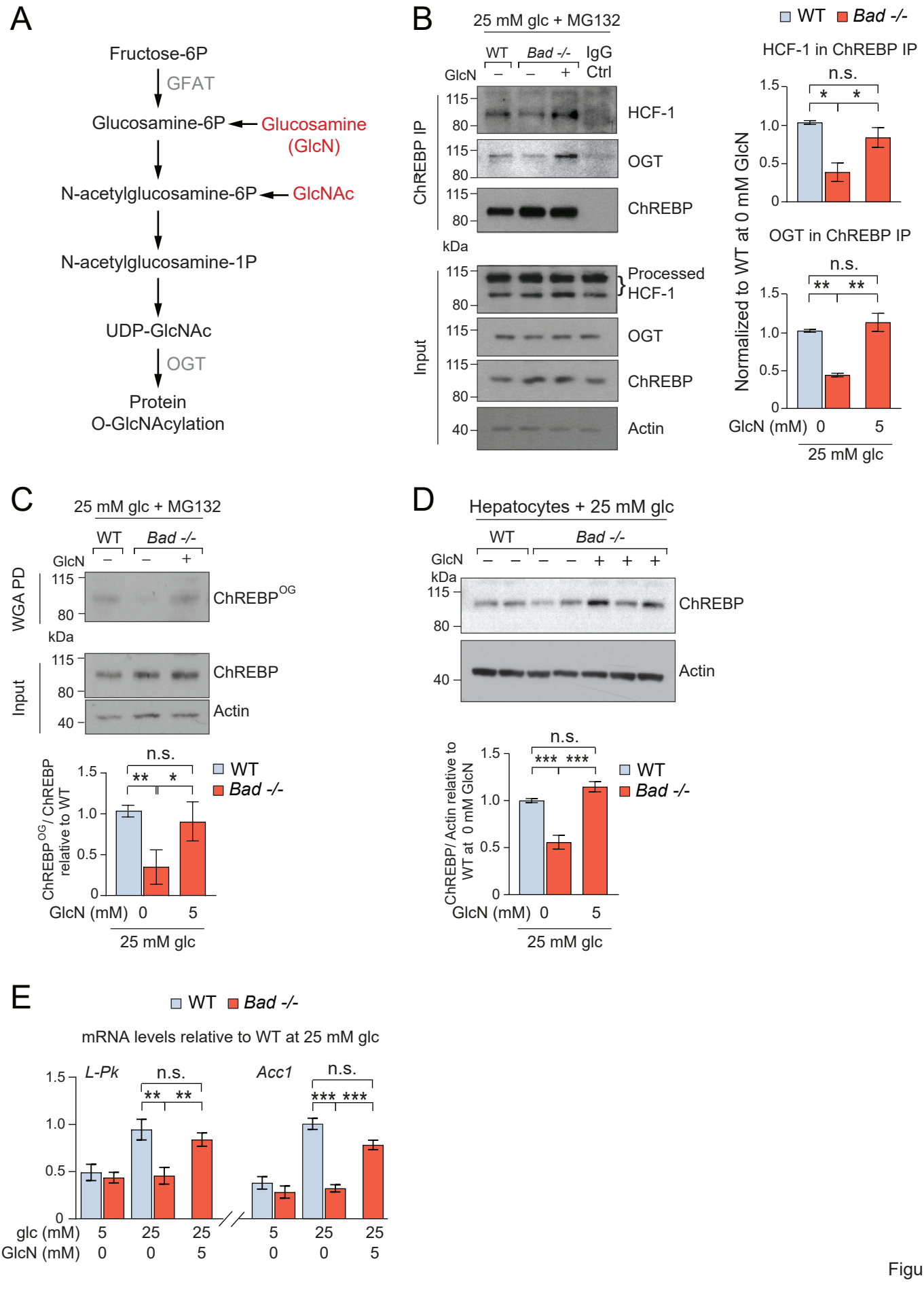
A
Fructose-6P
GFAT
Glucosamine-6P
Glucosamine (GlcN)
N-acetylglucosamine-6P
GlcNAc
N-acetylglucosamine-1P
UDP-GlcNAc
OGT
Protein O-GlcNAcylation
B
25 mM glc + MG132
WT
Bad -/-
IgG Ctrl
GlcN
ChREBP IP
HCF-1
OGT
ChREBP
kDa
Input
Processed HCF-1
Actin
WT
Bad -/-
HCF-1 in ChREBP IP
n.s.
OGT in ChREBP IP
Normalized to WT at 0 mM GlcN
GlcN (mM) 0 5
25 mM glc
C
25 mM glc + MG132
WGA PD
ChREBP^OG
Input
ChREBP
Actin
n.s.
ChREBP^OG / ChREBP relative to WT
GlcN (mM) 0 5
25 mM glc
D
Hepatocytes + 25 mM glc
ChREBP
Actin
n.s.
ChREBP/ Actin relative to WT at 0 mM GlcN
GlcN (mM) 0 5
25 mM glc
E
WT
Bad -/-
mRNA levels relative to WT at 25 mM glc
L-Pk
Acc1
n.s.
glc (mM) 5 25 25 5 25 25
GlcN (mM) 0 0 5 0 0 5

Figure S6

Figure S6, related to Figure 4. Modulation of the HCF-1-ChREBP regulatory module by hexosamine pathway metabolites

(A) Schematic of the hexosamine biosynthesis pathway.

(B) Representative western blots (left) and quantification of n=3 experiments (right) of ChREBP association with HCF-1 and OGT in WT and *Bad -/-* primary hepatocytes cultured in 25 mM glucose (glc) and 20 μM MG132 in the absence or presence of 5 mM GlcN for 6 hrs.

(C) Representative western blots (top) and quantification of n=3 experiments (bottom) of $ChREBP^{OG}$ in WGA pull down assays in WT and *Bad -/-* primary hepatocytes cultured as in (B)

(D) Representative western blots (top) and quantification of n=4 experiments (bottom) of ChREBP protein levels in WT and *Bad -/-* primary hepatocytes cultured as in (B).

(E) Relative expression of ChREBP target genes *L-Pk* and *Acc1* in WT and *Bad -/-* primary hepatocytes cultured in 5 or 25 mM glucose (glc) in the absence or presence of 5 mM GlcN for 8 hrs (n=9 experimental repeats in hepatocytes derived from 3 mice per genotype).

Error bars in B-E are means ± SEM, *p < 0.05; **p < 0.01; ***p < 0.001; n.s., non-significant; two way ANOVA (B, D-E) or one way ANOVA (C).

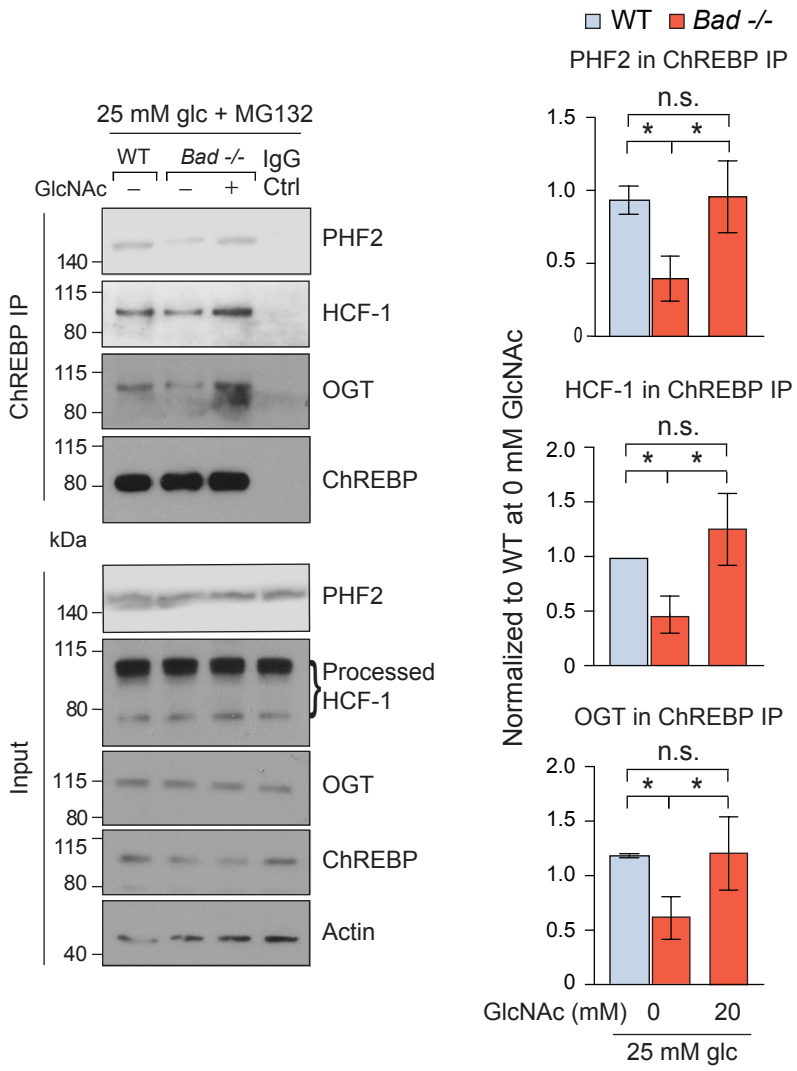
25 mM glc + MG132
WT
Bad -/-
IgG Ctrl
GlcNAc – – +
ChREBP IP
kDa
PHF2
HCF-1
OGT
ChREBP
Input
Processed HCF-1
Actin
140
115
80
40
WT
Bad -/-
PHF2 in ChREBP IP
HCF-1 in ChREBP IP
OGT in ChREBP IP
n.s.
*
Normalized to WT at 0 mM GlcNAc
1.5
1.0
0.5
0
2.0
GlcNAc (mM) 0 20
25 mM glc

Figure S7

Figure S7, related to Figure 5. Regulation of the ChREBP:PHF2 complex by hexosamine pathway metabolites

Representative western blots (left) and quantification of n=3 experiments (right) of ChREBP IP experiments shown in Figure 4C reblotted with an antibody to PHF2 to assess the integrity of the ChREBP:PHF2 transcriptional complex in WT vs *Bad* -/- hepatocytes and its regulation by hexosamine pathway metabolites.